Eur. Phys. J. C (2025) 85:1201
https://doi.org/10.1140/epjc/s10052-025-14952-x

THE EUROPEAN PHYSICAL JOURNAL C

Regular Article - Theoretical Physics

Rotating charged black holes in Kalb–Ramond gravity: electromagnetic fields, circular motion and collisions of charged particles

Shokhzod Jumaniyozov[1,a], **Javlon Rayimbaev**[2,3,4,b], **Yunus Turaev**[5,c], **Inomjon Ibragimov**[6,d], **Bakhrom Abdulazizov**[7,e], **Munisbek Akhmedov**[8,f], **Sherzod Djumanov**[9,g]

[1] New Uzbekistan University, Movarounnahr Street 1, Tashkent 100000, Uzbekistan
[2] Institute of Fundamental and Applied Research, National Research University TIIAME, Kori Niyoziy 39, Tashkent 100000, Uzbekistan
[3] University of Tashkent for Applied Sciences, Str. Gavhar 1, Tashkent 100149, Uzbekistan
[4] National University of Uzbekistan, Tashkent 100174, Uzbekistan
[5] Mamun University, Bolkhovuz Street 2, Khiva 220900, Uzbekistan
[6] Kimyo International University in Tashkent, Shota Rustaveli street 156, Tashkent 100121, Uzbekistan
[7] Faculty of Physics, Namangan State University, Bobur shoh Str. 161, Namangan 160107, Uzbekistan
[8] Department of Technique, Urgench State University, Kh. Alimjan Str. 14, Urgench 221100, Uzbekistan
[9] Tashkent State Technical University, Tashkent 100095, Uzbekistan

Received: 3 September 2025 / Accepted: 10 October 2025

Abstract In this study, we investigate the electromagnetic field properties of a rotating charged black hole (BH) within the Kalb–Ramond gravity, as well as the circular motion and collisions of test charged particles in the spacetime of the BH. First, the static solutions of the Kalb–Ramond BH are derived using modified Einstein field equations and Maxwell's equations to obtain the anisotropic solutions of the charged Kalb–Ramond BH. Then, using the Janis–Newman formalism, the exact solutions of the rotating Kalb–Ramond BH are obtained from the static metric. Subsequently, we investigate the horizon properties of the resulting rotating BH. It is shown that all the BH parameters charge and rotation, together with the Kalb–Ramond field, cause the horizon to extend, thereby providing additional gravitational mass. Then, we derive expressions for non-zero components of electromagnetic field configurations with respect to a zero angular momentum observer around the BHs. We also explore the circular motion of charged test particles, determining their effective potential and innermost stable circular orbits (ISCOs), which are influenced by the interplay of gravitational, rotational, and electromagnetic forces. Furthermore, we examine high-energy collisions of charged particles near the event horizon, computing the center-of-mass energy and demonstrating its enhancement by the Kalb–Ramond parameter and BH charge. Our results highlight the potential of charged rotating Kalb–Ramond BHs as natural particle accelerators, offering insights into extreme gravitational and electromagnetic phenomena with implications for astrophysics and theoretical physics.

1 Introduction

Einstein's general relativity (GR) provides a mathematically consistent framework for describing gravitational interactions as the curvature of spacetime induced by massive objects [1]. This theory has been extensively validated across a range of gravitational regimes, from weak-field tests, such as the perihelion precession of Mercury, to strong-field observations, including the imaging of BH shadows by the Event Horizon Telescope [2–4]. Despite its successes, the increasing precision of modern astrophysical observations, such as those from X-ray binaries and supermassive BHs, encourages the investigation of alternative and modified gravity theories to probe potential deviations from GR [5–7]. Among these, Kalb–Ramond (KR) gravity introduces a novel modification

[a] e-mail: sh.jumaniyozov@newuu.uz
[b] e-mail: javlon@astrin.uz (corresponding author)
[c] e-mail: yunus.turaev.nw@gmail.com
[d] e-mail: i.ibragimov@kiut.uz
[e] e-mail: abdulazizovbahromjon@gmail.com
[f] e-mail: munisbek95@urdu.uz
[g] e-mail: djumanov.sherzod1984@gmail.com

Published online: 25 October 2025

by incorporating a second-rank antisymmetric tensor field, which emerges naturally in the context of heterotic string theory [8–11]. This self-interacting field can lead to Lorentz-violating effects and contribute to spacetime torsion, offering a distinct perspective on gravitational dynamics [12–16].

The study of charged rotating BHs in KR gravity is particularly compelling due to the intricate interplay of gravitational, electromagnetic, and KR field effects. The presence of a background KR field modifies the spacetime metric, influencing the dynamics of charged particles and their circular orbits around such BHs [17–22]. These modifications can manifest in observable astrophysical phenomena, including the trajectories of test particles, high-energy particle collisions, and the radiation profiles of accretion disks [23–25]. Charged rotating BHs, analogous to the Kerr–Newman solution in GR, provide a rich environment for studying these effects, as their electromagnetic fields and spin introduce additional complexities to particle dynamics compared to uncharged or non-rotating cases [26–28].

BHs represent one of the most profound predictions of general relativity, serving as natural laboratories to probe the interplay between gravity, quantum fields, and exotic matter configurations. Among the numerous extensions of Einstein's theory, the KR field, a rank-2 antisymmetric tensor field derived from string theory, provides a compelling framework for exploring deviations from classical gravitation. The KR field, characterized by the tensor $B_{\alpha\beta}$ with an antisymmetric property ($B^{\alpha\beta} = -B^{\beta\alpha}$), introduces a nontrivial vacuum expectation value $< B_{\mu\nu} >= b_{\mu\nu} \neq 0$, leading to a field strength $H_{\alpha\beta\gamma} = \partial_{[\alpha} B_{\beta\gamma]}$ analogous to the electromagnetic field tensor. This similarity allows the KR action to be formulated in a manner reminiscent of electrodynamics, coupled non-minimally to gravity through terms involving the Ricci curvature tensor $R_{\mu\nu}$ and scalar R [29,30]. The resulting gravitational action, incorporating the KR field and its potential $V(B^{\mu\nu}B_{\mu\nu} \pm b^2)$, provides a rich landscape to investigate BH solutions and their physical implications.

The study of BHs in KR gravity has gained significant traction due to their potential to address unresolved questions in cosmology and astrophysics, such as the nature of dark matter and the behavior of particles in extreme gravitational environments [31–34]. In this context, charged and rotating BH solutions within KR gravity offer a unique opportunity to explore how the KR field modifies space-time geometry and influences physical processes near the event horizon. The action governing such systems is given by:

$$S_{\rm KR} = \frac{1}{2}\int d^4x\,\sqrt{-g}\Big[R - \frac{1}{6}H_{\mu\nu\sigma}H^{\mu\nu\sigma} - V(B^{\mu\nu}B_{\mu\nu} \pm b^2) + \xi_2 B^{\sigma\mu}B^{\nu}_{\mu}R_{\sigma\nu} + \xi_3 B^{\mu\nu}B_{\mu\nu}R\Big], \tag{1}$$

where, g represents the determinant of the metric tensor, $R_{\mu\nu}$ refers to the Ricci curvature tensor, and R denotes the Ricci curvature scalar. The potential V is related to the previously mentioned vacuum expectation value of the tensor field $B_{\mu\nu}$, while ξ_2 and ξ_3 indicate the constants associated with non-minimal coupling [35,36].

As noted earlier, the KR field can impact particles, making it worthwhile to explore their motion and collisions when the KR field is present. Given that we are examining the gravitational properties of the KR field, it becomes intriguing to investigate particle collisions near a BH within this field [35,37]. These collisions release energy, which can be quantified using the energy of the center of mass, as the moving particles possess momentum and, consequently, energy [38]. Such BHs are referred to as particle accelerators. Numerous studies on this topic can be found [39–41].

This work investigates the circular motion of charged particles and their collision processes in the vicinity of a charged rotating BH within a KR gravitational framework. We aim to analyze the effects of the BH's charge, spin, and KR field parameters on orbital dynamics, energy profiles, and collision outcomes. By employing analytical and numerical techniques, we explore geodesic motion, effective potentials, and the stability of circular orbits, drawing comparisons with standard Kerr and Reissner–Nordström solutions [42–44]. Additionally, we examine the implications of particle collisions for energy extraction mechanisms, such as the Penrose process, and their potential observational signatures in accretion disk emissions [45–52]. Our study aims to connect theoretical predictions with astrophysical observations, thereby providing constraints on the parameters of KR gravity and paving the way for testing modified gravity theories in extreme gravitational environments.

The organization of this manuscript is as follows: Sect. 2 examines the spacetime features surrounding BHs in KR gravity. In Sect. 3, we examine the effects of our given parameters on the event horizon and ergosphere radii. In Sect. 4, we investigate the characteristics of the electromagnetic field components surrounding the BH under consideration. Our analysis encompasses a detailed exploration of the spatial and temporal properties of these field components, aiming to elucidate their behavior, interactions, and underlying physical implications within the context of the BH's environment. Section 5 is dedicated to studying the circular motion of charged test particles. In Sect. 6, we conduct an in-depth analysis of particle collisions, examining their dynamics, energy exchanges, and the resulting trajectories to gain a deeper understanding of the fundamental principles governing these interactions. Finally, Sect. 7 summarizes our results and offers concluding observations. We use a spacetime metric signature of $(-,+,+,+)$ and operate within a geometrized unit system where $G = c = 1$. Latin indices span from 1 to 3, while the Greek indices span from 0 to 3.

2 Charged rotating BH in Kalb–Ramond gravity

In this section, we derive the spacetime metric of the charged rotating BH in KR gravity. This process involves connecting the interplay between the gravitational, electromagnetic, and KR fields, transitioning to the rotating metric via the Janis-Newman method.

2.1 Static KR BH solution

In Eq. (1), the total action for the modified theory of gravity is introduced that explicitly incorporates spontaneous Lorentz symmetry-breaking (LSB) via a non-vanishing VEV of the KR field $B_{\mu\nu}$, a rank-2 antisymmetric tensor field naturally arising in string theory. The field strength remains unchanged under the gauge transformation $B_{\mu\nu} \rightarrow B_{\mu\nu} + \partial_{[\mu}\Gamma_{\nu]}$. It is useful to express the KR field as $B_{\mu\nu} = E_{[\mu}v_{\nu]} + \epsilon_{\mu\nu\alpha\beta}v^{\alpha}\tilde{B}^{\beta}$, where $E_{\mu}v^{\mu} = 0$ and $\tilde{B}_{\mu}v^{\mu} = 0$, and v^{α} is a timelike 4-vector. Consequently, the spacelike pseudo-vector fields E_{μ} and $\tilde{B}_{\mu}$ can be understood as analogous to the pseudo-electric and pseudo-magnetic fields, respectively, like Maxwell's electrodynamics. To obtain charged solutions, we define the matter Lagrangian $\mathcal{L}_M$ as the electromagnetic field, expressed as $\mathcal{L}_M = -\frac{1}{2}F_{\mu\nu}F^{\mu\nu} + \mathcal{L}_{\text{int}}$, where $F_{\mu\nu} = \partial_{\mu}A_{\nu} - \partial_{\nu}A_{\mu}$ denotes the electromagnetic field strength, and $\mathcal{L}_{\text{int}}$ describes the interaction between the electromagnetic field and the KR field. The potential $V(B_{\mu\nu}B^{\mu\nu} \pm b^2)$ is constructed to depend on $B_{\mu\nu}B^{\mu\nu}$ to preserve the theory's invariance under local Lorentz transformations for observers. Since the cosmological constant Λ is treated separately, the potential is set to vanish at its minimum, which occurs when $B_{\mu\nu}B^{\mu\nu} = \mp b^2$, with the sign $\pm$ chosen to ensure b^2 is positive. As a result, the KR field develops a nonzero VEV, denoted as $\langle B_{\mu\nu}\rangle = b_{\mu\nu}$. Due to the non-minimal coupling of the KR field to gravity, this nonzero VEV $b_{\mu\nu}$ spontaneously breaks local Lorentz invariance for particles. In the vacuum state, the interaction term $\xi_3 B_{\mu\nu}B^{\mu\nu}R = \mp\xi_3 b^2 R$ in the action (1) can be incorporated into the Einstein–Hilbert terms through a redefinition of variables. Additionally, we assume that the only nonzero components of the vacuum configuration of the KR field are given by

$$b_{10} = -b_{01} = \tilde{E}(r), \tag{2}$$

as described in Ref. [53]. As a result, this configuration inherently leads to the vanishing of the KR field strength, i.e., $H_{\lambda\mu\nu} = 0$. To obtain electrically charged BH solutions, we adopt an electrostatic vector potential $A_{\mu} = -\Phi(r)\delta^{t}_{\mu}$ in the standard approach. However, it is crucial to recognize that a consistently charged BH solution cannot be sustained by the electromagnetic field alone without the interaction term $\mathcal{L}_{\text{int}}$. To account for this interaction, one method is to modify the KR field strength $H_{\mu\nu\rho}$ by including a $U(1)$ electromagnetic Chern–Simons three-form, such that $\tilde{H}_{\mu\nu\rho} = H_{\mu\nu\rho} + A_{[\mu}F_{\nu\rho]}$. However, for the vacuum KR configuration Eq.(2) and the electrostatic vector potential, the interactions in the modified kinetic term $\tilde{H}_{\mu\nu\rho}\tilde{H}^{\mu\nu\rho} = H_{\mu\nu\rho}H^{\mu\nu\rho} + 2H_{\mu\nu\rho}A_{[\mu}F_{\nu\rho]} + A_{[\mu}F_{\nu\rho]}A^{[\mu}F^{\nu\rho]}$ are found to vanish. Thus, to introduce a nontrivial contribution to the spacetime dynamics, we consider the Lagrangian in the form

$$\mathcal{L}_M = -\frac{1}{2}F_{\mu\nu}F^{\mu\nu} - \eta B^{\alpha\beta}B^{\gamma\rho}F_{\alpha\beta}F_{\gamma\rho}, \tag{3}$$

where η is a coupling parameter mediating the LSB in the gauge sector. When the KR field develops a nonzero VEV, the Lagrangian leads to LSB in the electromagnetic field, enabling the existence of electrically charged BH solutions. The modified Einstein equations are derived by varying the action (1) with respect to the metric $g_{\mu\nu}$, resulting as follows

$$R_{\mu\nu} - \frac{1}{2}g_{\mu\nu}R = T^{\text{M}}_{\mu\nu} + T^{\text{KR}}_{\mu\nu}, \tag{4}$$

where $T^{M}_{\mu\nu}$ represents the energy–momentum tensor of the electromagnetic field, obtained as

$$\begin{aligned} T^{M}_{\mu\nu} &= 2F_{\mu\alpha}F_{\nu}{}^{\alpha} - \frac{1}{2}g_{\mu\nu}F^{\alpha\beta}F_{\alpha\beta} \\ &\quad + \eta\left(8B^{\alpha\beta}B_{\nu\gamma}F_{\alpha\beta}F_{\gamma\eta} - g_{\mu\nu}B^{\alpha\beta}B^{\gamma\delta}F_{\alpha\beta}F_{\gamma\delta}\right), \end{aligned} \tag{5}$$

and $T^{KR}_{\mu\nu}$ is the effective energy-momentum tensor of the KR field, given by

$$\begin{aligned} T^{KR}_{\mu\nu} &= \frac{1}{2}H_{\mu\alpha\beta}H^{\alpha\beta}_{\nu} - \frac{1}{12}g_{\mu\nu}H^{\alpha\beta\rho}H_{\alpha\beta\rho} + 2V'B_{0\mu}B^{\alpha}_{\nu} - g_{\mu\nu}V \\ &\quad + \xi_2\Bigg[\frac{1}{2}g_{\mu\beta}B^{\gamma\beta}R_{\alpha\beta} = B^{\mu\beta}B^{\nu}_{\beta}R_{\alpha\beta} - B^{\alpha\beta}B_{\nu\beta}R_{\mu\alpha} \\ &\quad - B^{\alpha\beta}B_{\mu\beta}R_{\nu\alpha} + \frac{1}{2}\nabla_{\alpha}\nabla_{\mu}(B^{\alpha\beta}B_{\nu\beta}) + \frac{1}{2}\nabla_{\alpha}\nabla_{\nu}(B^{\alpha\beta}B_{\mu\beta}) \\ &\quad - \frac{1}{2}\nabla_{\alpha}\nabla_{\alpha}(B_{\mu\gamma}B_{\nu\gamma}) - \frac{1}{2}g_{\mu\nu}\nabla_{\alpha}\nabla_{\beta}(B^{\gamma\beta}B^{\beta}_{\gamma})\Bigg]. \end{aligned} \tag{6}$$

In this context, the prime denotes the derivative with respect to the argument of the respective functions. It is worth noting that the total energy-momentum tensor $T^{\text{KR}}_{\mu\nu} + T^{\text{M}}_{\mu\nu}$ is conserved due to the Bianchi identities. The equation of motion for the KR field is derived by varying the action (1) with respect to $B_{\mu\nu}$, and can be written as

$$\nabla^{\alpha}H_{\alpha\mu\nu} + 3\xi R_{\alpha[\mu}B^{\alpha}{}_{\nu]} - 6V'B_{\mu\nu} - 12\eta B^{\alpha\beta}F_{\alpha\beta}F_{\mu\nu} = 0. \tag{7}$$

Additionally, the modified Maxwell equation is obtained by varying the action (1) with respect to the vector potential A_μ, resulting in

$$\nabla^\nu \left(F_{\mu\nu} + 2\eta B_{\mu\omega} B^{\alpha\beta} F_{\alpha\beta}\right) = 0. \tag{8}$$

It simplifies to the conventional Maxwell equation when the coupling constant η is set to zero. We consider the metric ansatz for a static and spherically symmetric spacetime given by

$$ds^2 = -f(r)dt^2 + g(r)dr^2 + r^2(d\theta^2 + \sin^2\theta d\phi^2), \tag{9}$$

Using the ansatz, the function $\tilde{E}(r)$ from (2) can be further written as $\tilde{E}(r) = |b|\sqrt{\frac{f(r)g(r)}{2}}$. As a result, the vacuum configuration of the KR field adheres to the constant norm condition $b_{\mu\nu}b^{\mu\nu} = -b^2$. In the vacuum configuration, it is beneficial to reframe the modified Einstein equation (4) as

$$\begin{aligned} R_{\mu\nu} = {} & T^M_{\mu\nu} - \frac{1}{2}g_{\mu\nu}T^M + V'\left(2b_{\mu\alpha}b^\alpha_\nu + b^2 g_{\mu\nu}\right) \\ & + \xi_2\Big[g_{\mu\nu}b^{\alpha\gamma}b^\beta_\gamma R_{\alpha\beta} - b^\alpha_\mu b^\beta_\nu R_{\alpha\beta} \\ & - b^{\alpha\beta}b_{\mu\beta}R_{\nu\alpha} - b^{\alpha\beta}b_{\nu\beta}R_{\mu\alpha} \\ & + \frac{1}{2}\nabla_\alpha\nabla_\mu\left(b^{\alpha\beta}b_{\nu\beta}\right) + \frac{1}{2}\nabla_\alpha\nabla_\nu\left(b^{\alpha\beta}b_{\mu\beta}\right) \\ & - \frac{1}{2}\nabla^\alpha\nabla_\alpha\left(b^\gamma_\mu b_{\nu\gamma}\right)\Big]. \end{aligned} \tag{10}$$

where $T^M \equiv g^{\alpha\beta}T^M_{\alpha\beta}$. Moreover, using the ansatzes for the metric (25) and the electrostatic field, the field equations (10) can be explicitly expressed as

$$\frac{2f''}{f} - \frac{f'g'}{fg} - \frac{f'^2}{f^2} + \frac{4f'}{rf} + \frac{4g'}{rg} - \frac{4(1-2\eta b^2)\Phi'^2}{(1-l)f} = 0, \tag{11}$$

$$\frac{2f''}{f} - \frac{f'g'}{fg} - \frac{f'^2}{f^2} - \frac{4g'}{rg} - \frac{4(1-2\eta b^2)\Phi'^2}{(1-l)f} = 0, \tag{12}$$

$$\begin{aligned} & \frac{2f''}{f} - \frac{f'g'}{fg} - \frac{f'^2}{f^2} + \frac{1+l}{lr}\left(\frac{f'}{f} - \frac{g'}{g}\right) + \frac{2(1-l)}{lr^2} \\ & - (1-b^2r^4V')\frac{2g}{lr^2} - \frac{2(1-6\eta b^2)\Phi^2}{lf} = 0, \end{aligned} \tag{13}$$

where $l \equiv \xi_2 b^2/2$, known as the Lorentz-violating parameter, quantifies the extent of Lorentz-breaking effects. Additionally, the field equation for the KR field (7) and the modified Maxwell equation (8) are expressed explicitly as

$$\frac{2f''}{f} - \frac{f'^2}{f^2} + \frac{2}{r}\left(\frac{f'}{f} - \frac{g'}{g}\right) - \frac{f'}{f}\frac{g'}{g} + \frac{2b^2V'g}{l} - \frac{8\eta b^2\Phi^2}{lf} = 0, \tag{14}$$

$$(1-2\eta b^2)\left[\Phi'' + \frac{\Phi'}{2}\left(\frac{4}{r} - \frac{f'}{f} - \frac{g'}{g}\right)\right] = 0. \tag{15}$$

When the cosmological constant is absent, we assume $V' = 0$, which applies to the scenario where the VEV lies at the potential's local minimum. This can be easily achieved with a quadratic potential, $V = \frac{1}{2}\lambda X^2$, where $X \equiv B_{\mu\nu}B^{\mu\nu} + b^2$ and λ is a coupling constant. By subtracting Eq. (12) from Eq. (11), we obtain the following relationship:

$$\frac{f'}{f} = -\frac{g'}{g}. \tag{16}$$

It simply yields $g(r) = f^{-1}(r)$ where we have set the integration constant to 1, achievable by rescaling the time t in the metric (25). By substituting it into the modified Maxwell equation (15), we have

$$\Phi'' + \frac{2}{r}\Phi' = 0. \tag{17}$$

However, since the conserved current is now modified to $J_\mu = \nabla_\nu F^{\mu\nu} + 2\eta B_{\mu\nu}B^{\alpha\beta}F_{\alpha\beta}$, the electric charge Q can be calculated using Stokes's theorem, i.e.,

$$\begin{aligned} Q &= -\frac{1}{4\pi}\int_\Sigma dx^3\sqrt{(\gamma^3)}\eta_\mu J^\mu \\ &= -\frac{1}{4\pi}\int_{\partial\Sigma} d\theta d\phi\sqrt{(\gamma^2)}\eta_\mu\sigma_\nu\left(F^{\mu\nu} + 2\eta B^{\mu\nu}B^{\alpha\beta}F_{\alpha\beta}\right) \\ &= (1-2b^2\eta)\,c_1, \end{aligned} \tag{18}$$

where Σ represents a 3-dimensional spacelike region with the induced metric $\gamma^{(3)}_{ij}$, and its boundary $\partial\Sigma$ is a two-sphere at spatial infinity with the induced metric $\gamma^{(2)}_{ij} = r^2d\theta^2 + \sin^2\theta d\phi^2$. Accordingly, $n_\mu = (1,0,0,0)$ is the unit normal vector associated with Σ, and $\sigma_\mu = (0,1,0,0)$ is the unit normal vector associated with $\partial\Sigma$. Consequently, the integration constant c_1 is determined as $c_1 = Q/(1-2b^2\eta)$. Thus, the electrostatic potential is given by

$$\Phi(r) = \frac{Q}{(1-2b^2\eta)r}. \tag{19}$$

After subtracting Eq. (13) from Eq. (11) and inserting Eqs. (16) and (23) into the result, one obtains

$$\frac{f'}{f} + \frac{1+l-2(3-l)\eta b^2}{(1-l)^2(1-2\eta b^2)^2}\frac{Q^2}{r^3 f} - \frac{1}{(1-l)rf} + \frac{1}{r} = 0. \tag{20}$$

Subsequently, the metric function $f(r)$ can be determined through integration, leading to

$$f(r) = \frac{1}{1-l} - \frac{2M}{r} + \frac{1+l-2(3-l)\eta b^2 Q^2}{(1-l)^2(1-2\eta b^2)^2}\frac{1}{r^2}. \quad (21)$$

Moreover, by plugging the derived results into all the field equations (11)–(15), it is determined that the solutions are consistent only if

$$\eta = \frac{l}{2b^2}. \quad (22)$$

Hence, it is clear that, in the presence of Lorentz violation in spacetime, the interaction term $\mathcal{L}_{\text{int}}$ is essential to obtain a charged BH solution. Using the relation (22), the electrostatic potential $\Phi(r)$ and the metric function $f(r)$ can be further streamlined as

$$\Phi = \frac{Q}{(1-l)r} \quad (23)$$

$$f(r) = 1/g(r) = \frac{1}{1-l} - \frac{2M}{r} + \frac{Q^2}{(1-l)^2 r^2}. \quad (24)$$

We note that the metric of the charged non-rotating KR BH, derived through the field equations, found a spherically symmetric solution, in the following form:

$$ds^2 = -f(r)dt^2 + g(r)dr^2 + h(r)(d\theta^2 + \sin^2\theta d\phi^2), \quad (25)$$

with the radial functions $f(r)$ and $h(r)$ as follows:

$$f(r) = \frac{1}{g(r)} = \frac{1}{1-l} - \frac{2M}{r} + \frac{Q^2}{(1-l)^2 r^2}; \quad h(r) = r^2, \quad (26)$$

where M is the BH mass, Q is the electric charge of the BH, and l modifies the gravitational potential due to the KR field's vacuum expectation value. This solution reduces to the Reissner–Nordström metric when $l = 0$ and to the Schwarzschild metric when both $l = 0$ and $Q = 0$.

2.2 Janis–Newman algorithm

Now, we use to the Janis–Newman method, to initiate the algorithm, transforming the spacetime metric given in Eq. (25) from Boyer–Lindquist coordinates (t, r, θ, ϕ) to Eddington–Finkelstein coordinates (u, r, θ, ϕ) through the following coordinate change [54,55]:

$$du = dt - \frac{dr}{f(r)}. \quad (27)$$

Applying this transformation leads to the spacetime metric taking the following form [56]:

$$ds^2 = -f du^2 - 2\sqrt{\frac{f}{g}} du dr + h(d\theta^2 + \sin^2\theta d\phi^2). \quad (28)$$

The contravariant components of the metric tensor in advanced null Eddington–Finkelstein coordinates can be represented in terms of the null tetrad as follows [57,58]:

$$g^{\mu\nu} = -l^\mu n^\nu - l^\nu n^\mu + m^\mu \bar{m}^\nu + m^\nu \bar{m}^\mu, \quad (29)$$

with

$$l^\mu = \delta^\mu_r = (0, 1, 0, 0), \quad (30)$$

$$n^\mu = \sqrt{\frac{g}{f}}\delta^\mu_u - \frac{f(r)}{2}\delta^\mu_r = \left(1, -\frac{f(r)}{2}, 0, 0\right), \quad (31)$$

$$m^\mu = \frac{1}{\sqrt{2r^2}}\delta^\mu_\theta + \frac{i}{\sqrt{2r^2}\sin\theta}\delta^\mu_\phi \quad (32)$$

$$= \left(0, 0, \frac{1}{r\sqrt{2}}, \frac{i}{r\sqrt{2}\sin\theta}\right), \quad (33)$$

$$\bar{m}^\mu = \frac{1}{\sqrt{2r^2}}\delta^\mu_\theta - \frac{i}{\sqrt{2r^2}\sin\theta}\delta^\mu_\phi \quad (34)$$

$$= \left(0, 0, \frac{1}{r\sqrt{2}}, -\frac{i}{r\sqrt{2}\sin\theta}\right). \quad (35)$$

Vectors l and n are real, m is a complex vector, $\bar{m}$ is the complex conjugate of the vector m.

These vectors satisfy orthogonality $l^\mu m_\mu = l^\mu \bar{m}_\mu = n^\mu m_\mu = n^\mu \bar{m}_\mu = 0$, isotropy $l^\mu l_\mu = n^\mu n_\mu = m^\mu m_\mu = \bar{m}^\mu \bar{m}_\mu = 0$, and normalization $l^\mu n_\mu = 1$, $m^\mu \bar{m}_\mu = -1$ conditions. The complex coordinate transformation used in the Janis-Newman algorithm is given by:

$$x'^\mu = x^\mu - ia(\delta^\mu_t - \delta^\mu_r)\cos\theta, \quad (36)$$

which leads to the following transformations for the coordinates:

$$\begin{cases} u' = u - ia\cos\theta, \\ r' = r + ia\cos\theta, \\ \theta' = \theta, \\ \phi' = \phi. \end{cases} \quad (37)$$

It is assumed that, following these transformations, the metric functions are modified accordingly: $f(r) \to F(r, a, \theta)$, $g(r) \to G(r, a, \theta)$, and $h(r) \to \Sigma(r, a, \theta)$. When $a = 0$,

these new functions revert to their original forms. Additionally, the null tetrads also acquire a new form:

$$l^\mu = \delta^\mu_r, \tag{38}$$

$$n^\mu = \sqrt{\frac{G}{F}}\delta^\mu_u - \frac{1}{2}F\delta^\mu_r, \tag{39}$$

$$m^\mu = \frac{1}{\sqrt{2\Sigma}}\left[\delta^\mu_\theta + ia\sin\theta\left(\delta^\mu_u - \delta^\mu_r\right) + \frac{i}{\sin\theta}\delta^\mu_\phi\right], \tag{40}$$

$$\bar{m}^\mu = \frac{1}{\sqrt{2\Sigma}}\left[\delta^\mu_\theta - ia\sin\theta\left(\delta^\mu_u - \delta^\mu_r\right) - \frac{i}{\sin\theta}\delta^\mu_\phi\right]. \tag{41}$$

By applying the specified null-tetrad values, the metric of the rotating BH in the Eddington–Finkelstein coordinate system can be constructed

$$\begin{aligned} ds^2 = {} & Fdu^2 + 2dudr + 2a\sin^2\theta[(1-F)dud\phi - drd\phi] \\ & - \Sigma d\theta^2 - \sin^2\theta(a^2\sin^2\theta(1-F) + \Sigma)d\phi^2. \end{aligned} \tag{42}$$

This setup represents a rotating BH when transformed into the Boyer–Lindquist coordinate system, a process accomplished through the application of a global coordinate transformation

$$du = dt + G(r)dr, \quad d\phi = d\phi' + F(r)dr \tag{43}$$

with

$$G(r) = -\frac{r^2+a^2}{f(r)r^2+a^2}, \quad F(r) = -\frac{a}{f(r)r^2+a^2}. \tag{44}$$

Lastly, we have

$$\Delta = a^2 - 2Mr + \frac{r^2}{1-l} + \frac{Q^2}{(1-l)^2}, \tag{45}$$

$$\Sigma = r^2 + a^2\cos^2\theta. \tag{46}$$

After transitioning to Boyer–Lindquist coordinates, the resulting metric matches Eq. (25), confirming the rotating charged KR BH spacetime[59]:

$$\begin{aligned} ds^2 = {} & -\left(\frac{\Delta - a^2\sin^2\theta}{\Sigma}\right)dt^2 + \frac{\Sigma}{\Delta}dr^2 + \Sigma d\theta^2 \\ & + \frac{\sin^2\theta}{\Sigma}\left[(r^2+a^2)^2 - \Delta a^2\sin^2\theta\right]d\phi^2 \\ & - 2a\sin^2\theta\left(\frac{r^2+a^2-\Delta}{\Sigma}\right)dtd\phi, \end{aligned} \tag{47}$$

where

$$\Delta = a^2 - 2Mr + \frac{r^2}{1-l} + \frac{Q^2}{(1-l)^2} \tag{48}$$

$$\Sigma = r^2 + a^2\cos^2\theta. \tag{49}$$

This derivation validates the metric used in our analysis, demonstrating how the KR field parameter l, charge Q, and rotation a emerge naturally from the underlying action. The presence of l introduces a deviation from classical general relativity, enhancing the gravitational and electromagnetic effects, which we explore further in subsequent sections on particle dynamics and collisions. Specifically, in the context of the charged KR BH, the analysis of the shadow radius of Sagittarius A* by the Event Horizon Telescope (EHT) Collaboration constrains l to the interval $-4.59 \times 10^{-3} \leq l \leq 1.24 \times 10^{-1}$ [60]. Additionally, further studies of time-like and light-like geodesics, including the precession of the S2 star and geodesic precession around the Earth, refine this constraint to $-0.185022 \leq l \leq 0.0609$. These bounds indicate that l is typically small and positive or slightly negative, ensuring that $1 - l$ remains positive in the metric and field expressions. The plots in the document (e.g., Figures for event horizon and ergosphere) use l values up to 0.4, which exceed the observational constraint of 0.0609. This discrepancy suggests that the plotted values may be exploratory or illustrative rather than strictly physically allowed based on current data. To address this, we acknowledge that $l = 0.4$ lies outside the EHT-derived bound and could imply a hypothetical scenario where the KR field's influence is significantly stronger than observed. Such values are useful for studying the qualitative behavior of the system, but should be interpreted with caution. The consequences of l approaching 1 include a potential breakdown of the solution, where the horizon structure and electromagnetic fields become ill-defined, potentially leading to a naked singularity or unphysical behavior. This limit warrants further theoretical investigation to establish the maximum allowable l beyond which the KR BH solution becomes non-viable.

3 Event horizon and ergosphere in KR gravity

The event horizon and ergosphere are critical features of a rotating BH, defining the boundaries of causal influence and frame-dragging effects. In the context of a charged rotating BH in KR gravity, these regions are modified by the BH's mass M, charge Q, spin parameter a, and the KR parameter l. Here, we analyze their properties based on the spacetime metric presented in Sect. 2, focusing on their dependence on Q, a, and l, and their implications for the dynamics of charged particles.

3.1 Event horizon

The event horizon is the surface where the radial metric component diverges $g^{rr} = 0$, corresponding to the roots of the function $\Delta = 0$. Solving $\Delta = 0$ yields the event horizon

radii:

$$r_{\pm} = M \pm \sqrt{M^2 - a^2(1-l) - \frac{Q^2}{1-l}}, \tag{50}$$

Where r_+ is the outer event horizon (the boundary of the BH), and r_- is the inner (Cauchy) horizon. The KR parameter l modifies the effective gravitational and electromagnetic contributions, with the terms $\frac{r^2}{1-l}$ and $\frac{Q^2}{(1-l)^2}$ amplifying the radial dependence compared to the standard Kerr–Newman case.

In Fig. 1, the graphical illustration of the outer event horizon radius r_+ for a charged rotating BH in KR gravity, as a function of the BH charge Q, spin parameter a, and Lorentz-violating KR parameter l. The left panel shows the variation of r_+ concerning Q/M for fixed $a/M = 0.3$ and varying $l \in [-0.4, 0.4]$, demonstrating that increasing Q reduces r_+, with a positive l further shrinking the horizon. The middle panel illustrates r_+ as a function of a/M for fixed $Q/M = 0.5$, showing that higher spin decreases r_+, with the effect amplified by positive l. The right panel depicts r_+ versus l for fixed $Q/M = 0.5$ and $a/M = 0.3$, highlighting that r_+ decreases as l increases, reflecting the KR field's enhancement of electromagnetic and gravitational effects. For example, at $Q/M = 0.5$, $a/M = 0.3$, and $l = 0.03$, $r_+ \approx 1.6M$, compared to $r_+ \approx 1.95M$ in the Kerr case.

3.2 Ergosphere

The ergosphere is the region where the spacetime metric component g_{tt} changes sign, indicating that observers cannot remain stationary due to frame dragging. The boundary of the ergosphere, known as the ergosurface, is determined by $g_{tt} = 0$. Solving for r, the ergosurface radius is:

$$r_{\text{ergo}} = M \pm \sqrt{M^2 - \frac{a^2}{1-l}(1 - l\cos^2\theta) - \frac{Q^2}{(1-l)^2}}. \tag{51}$$

The ergosphere extends from the outer event horizon r_+ to the outer ergosurface, with its shape depending on the polar angle θ. The KR parameter l influences the ergosphere's extent through the terms $\frac{Q^2}{(1-l)^2}$ and $\frac{a^2}{1-l}$. A positive l reduces the ergosurface radius, compressing the ergosphere, while the charge Q further shrinks it due to the enhanced electromagnetic contribution.

In Fig. 2, a graphical illustration of the ergosphere radius r_{ergo} in the equatorial plane ($\theta = \pi/2$) for a charged rotating BH in KR gravity, as a function of the BH charge Q and KR parameter l. The left panel shows the dependence of r_{ergo} on Q/M for fixed $a/M = 0.3$ and varying $l \in [-0.4, 0.4]$, indicating that increasing Q compresses the ergosphere, with positive l enhancing this effect due to the amplified electromagnetic term $Q^2/(1-l)^2$. The right panel depicts r_{ergo} as a function of l for fixed $Q/M = 0.5$ and $a/M = 0.3$, demonstrating that a positive l reduces r_{ergo}, shrinking the ergosphere. For instance, at $Q/M = 0.5$, $a/M = 0.3$, and $l = 0.03$, $r_{\text{ergo}} \approx 2.1M$, compared to $r_{\text{ergo}} \approx 2.4M$ in the Kerr case. These shifts influence frame-dragging effects and the dynamics of test particles.

4 Electromagnetic field around rotating charged BH in KR gravity

The electromagnetic field surrounding a charged rotating BH in KR gravity emerges from the electric charge Q and the KR field parameter l, which collectively modify the spacetime geometry alongside the rotation parameter a. This section elucidates the configuration of the electromagnetic field through its vector potential A_μ, analyzing its properties using the Giampieri and tetrad formulations of the JN algorithm [61]. These approaches, inspired by Erbin's extensions of the JN method to gauge fields [62], are adapted to the KR framework, providing a robust framework for deriving the characteristics of the field.

In the JN tetrad formalism, the vector potential is computed in its contravariant form. Using the null tetrad basis $l^\mu = \delta^\mu_r, n^\mu, m^\mu$, and $\bar{m}^\mu$, the initial potential $A_\mu = \frac{Q}{(1-l)r}\delta^\mu_\mu$ is expressed as:

$$A^\mu = -\frac{Q}{(1-l)r} l^\mu. \tag{52}$$

Upon applying the complex transformation and the rule $r^{-1} \to \frac{r}{\Sigma}$, the transformed potential is:

$$A'^\mu = -\frac{Q}{(1-l)}\frac{r}{\Sigma}\delta^\mu_r. \tag{53}$$

In Boyer–Lindquist coordinates, the non-zero components of the vector potential for the charged rotating KR BH are expressed as:

$$A_t = -\frac{Q}{(1-l)}\frac{r}{\Sigma}, \tag{54}$$

$$A_\phi = \frac{Q}{(1-l)}\frac{r}{\Sigma} a\sin^2\theta, \tag{55}$$

where $\Sigma = r^2 + a^2\cos^2\theta$. The factor $(1-l)^{-1}$ arises from the coupling between the KR field and the electromagnetic sector, amplifying the potential compared to the Kerr–Newman case ($l = 0$) [63]. Here, A_t captures the electrostatic contribution, while A_ϕ reflects the frame-dragging effect induced by rotation, scaled by a.

The field tensor $F_{\mu\nu} = \partial_\mu A_\nu - \partial_\nu A_\mu$ yields key components, such as $F_{tr} = -\frac{Q}{(1-l)}\frac{r^2 - a^2\cos^2\theta}{\Sigma^2}$, which asymptot-

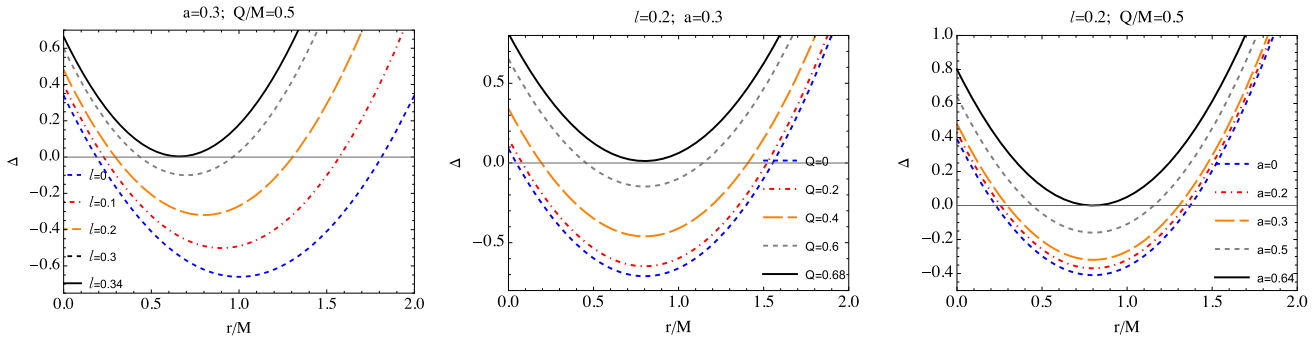

Fig. 1 Graphical illustration of the event horizon radius of a charged rotating BH in KR gravity for different parameter values Q, l, and a.

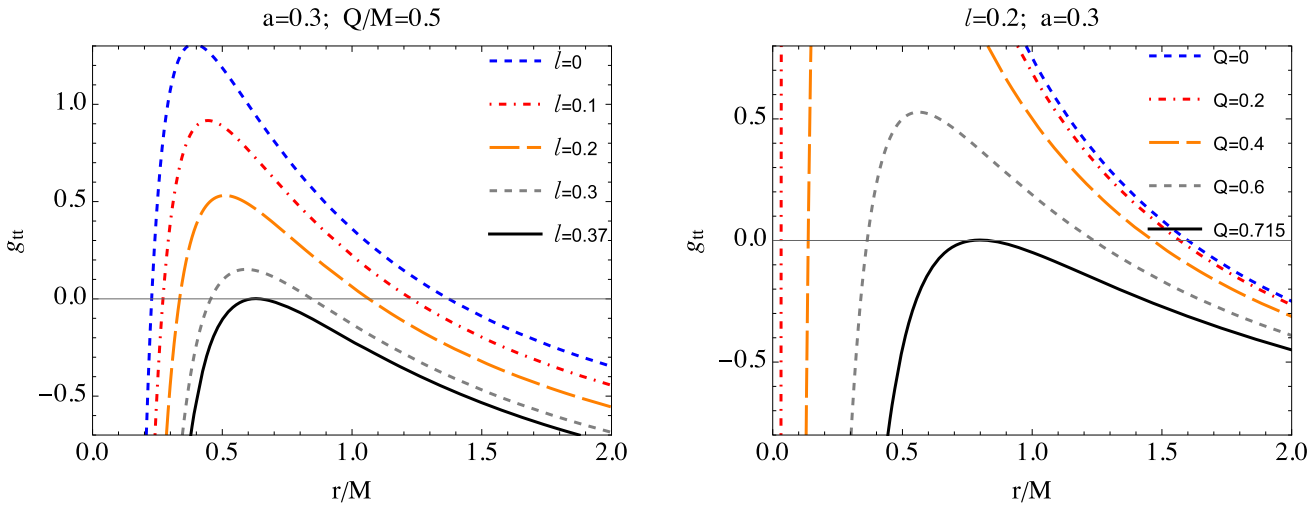

Fig. 2 Graphical illustration of the ergosphere radius of a charged rotating BH in KR gravity for different values of the parameter Q and l

ically approaches $\frac{Q}{(1-l)r^2}$ at large r, resembling a Coulomb field modified by l.

Tetrad methods offer an efficient means to calculate the electromagnetic field around a charged rotating KR BH, which is crucial for understanding charged particle dynamics and energy extraction processes. This approach leverages Erbin's advancements in extending the JN algorithm to gauge fields, thereby enriching the phenomenology of KR gravity. Subsequently, we leverage the Maxwell formalism in curved spacetime to calculate the electromagnetic field components surrounding the charged rotating BH in KR gravity. This approach allows us to systematically derive the electric and magnetic field vectors E^α and B^α. Specifically, these components are obtained from the electromagnetic field tensor $F_{\alpha\beta}$, which encapsulates the electromagnetic properties of spacetime and is evaluated relative to the four-velocity of ZAMO u^α. The ZAMO four-velocity in the equatorial plane ($\theta = \pi/2$) is $u^\alpha = (u^t, 0, 0, u^\phi)$, where $u^t = \sqrt{g_{\phi\phi}/(g_{t\phi}^2 - g_{tt}g_{\phi\phi})}$ and $u^\phi = -\frac{g_{t\phi}}{g_{\phi\phi}}u^t$. The electric field is defined as

$$E_\alpha = F_{\alpha\beta}u^\beta. \tag{56}$$

The electric field in the radial direction, where g^{rr} is the inverse radial metric component, and the terms $F_{rt}u^t$ and $F_{r\phi}u^\phi$ are taken into account to calculate radial and angular components of the field. Similarly, the electric field in the r and θ-direction is given by:

$$E^{\hat{r}} = \sqrt{(g^{rr})^3}\left(F_{rt}u^t + F_{r\phi}u^\phi\right) \tag{57}$$

$$E^{\hat{\theta}} = \sqrt{(g^{\theta\theta})^3}\left(F_{\theta\phi}u^\phi - F_{t\theta}u^t\right) \tag{58}$$

representing the projection of the field tensor onto the observer's timelike direction, while the magnetic field is given by

$$B^\alpha = \frac{1}{2}\eta^{\alpha\beta\sigma\mu}F_{\beta\sigma}u_\mu\,, \tag{59}$$

where the symbol $\eta_{\alpha\beta\sigma\gamma}$ is the pseudo-tensorial representation of the Levi-Civita symbol, denoted by $\epsilon_{\alpha\beta\sigma\gamma}$, and is characterized by the following form:

$$\eta_{\alpha\beta\sigma\gamma} = \sqrt{-g}\epsilon_{\alpha\beta\sigma\gamma}\,, \qquad \eta^{\alpha\beta\sigma\gamma} = -\frac{1}{\sqrt{-g}}\epsilon^{\alpha\beta\sigma\gamma}\,. \tag{60}$$

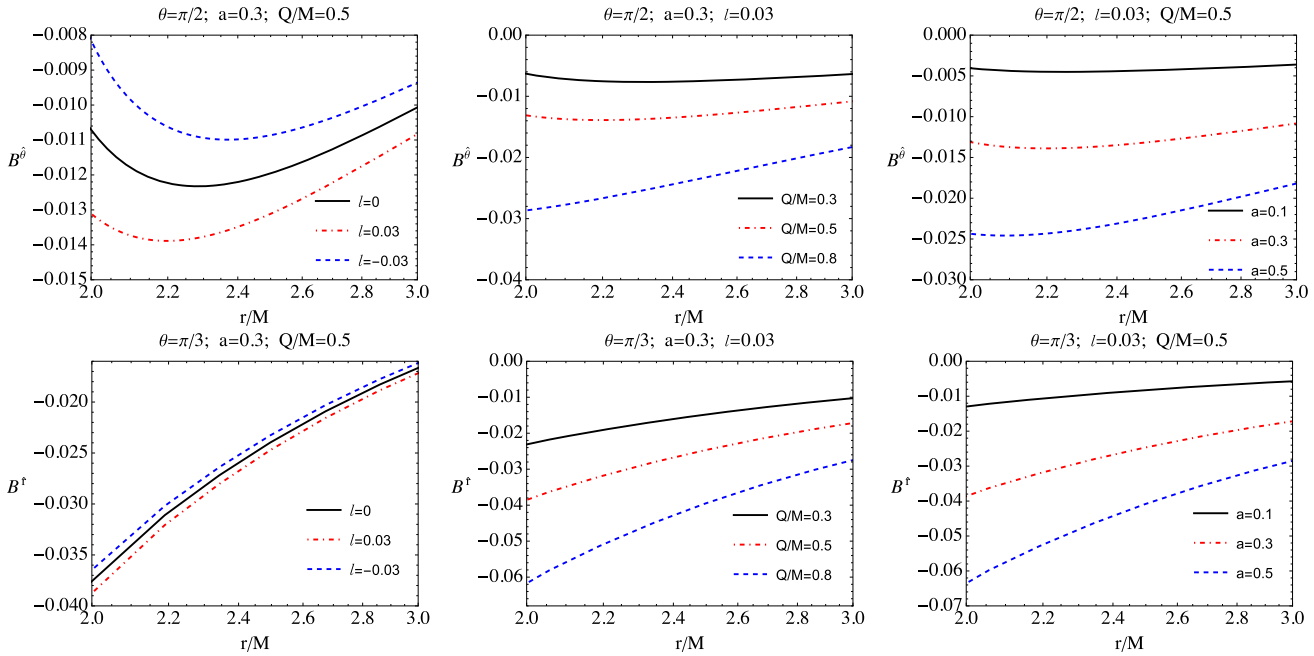

Fig. 3 Radial dependence of the magnetic field components $B^{\hat{\alpha}}$ around a charged rotating BH in KR gravity. Top row (left to right): $B^{\hat{\theta}}$ for $\theta = \pi/2$. Bottom row (left to right): $B^{\hat{r}}$ for $\theta = \pi/3$

with $g = det|g_{\mu\nu}|$. The magnetic field's components in an orthonormal coordinate system can be represented by utilizing the electromagnetic field tensor in the following form:

$$B^{\hat{i}} = \frac{1}{2}\epsilon_{ijk}\sqrt{g_{jj}g_{kk}}F^{jk} = \frac{1}{2}\epsilon_{ijk}\sqrt{g^{jj}g^{kk}}F_{jk}\ . \tag{61}$$

This expression describes the magnetic field along the radial direction in the orthonormal frame. Here, u_t is the time component of the four-velocity. The orthonormal components are crucial for understanding how the magnetic field behaves near the BH. The angular component of the magnetic field is similarly defined:

$$B^{\hat{r}} = \sqrt{-\frac{g_{rr}}{g}}F_{\theta\phi}u_t, \quad B^{\hat{\theta}} = -\sqrt{-\frac{g_{\theta\theta}}{g}}F_{r\phi}u_t. \tag{62}$$

The electromagnetic field in the presence of the charge of the BH Q, the rotation parameter a, and the KR field parameter l provides a comprehensive framework to explore their influence on the dynamics and the energy processes of charged particles. Now, by applying these expressions, we can quantify the field's behavior across different radial distances and assess its deviations from classical scenarios, such as the Kerr–Newman solution, thereby enriching our understanding of the KR gravity phenomenology.

The dependence of the components of the electric and magnetic fields on the radial coordinate is graphically illustrated in Figs. 3 and 4 for different values of the parameters Q, l, and a. In the left panel of Fig. 3, the magnetic field components $B^{\hat{r}}$ and $B^{\hat{\theta}}$ are shown for different values of the KR parameter. It can be inferred from the figure that as the KR parameter increases, the values of the magnetic field components decrease. In the middle panel of Fig. 3, the magnetic field components $B^{\hat{r}}$ and $B^{\hat{\theta}}$ are depicted for different values of the BH's charge. Here, too, as the charge increases, the values of the magnetic field components decrease. In the right panel of Fig. 3, the magnetic field components $B^{\hat{r}}$ and $B^{\hat{\theta}}$ are depicted for different values of the BH's spin parameter. It can also be inferred here that as the spin increases, the values of the magnetic field components decrease.

In the left panel of Fig. 4, the electric field components $E^{\hat{r}}$ and $E^{\hat{\theta}}$ are depicted for different values of the KR parameter. It can be inferred from the figure that as the KR parameter increases, the values of the electric field components $E^{\hat{r}}$ increase, while $E^{\hat{\theta}}$ decreases. In the middle panel of Fig. 4, the electric field components $E^{\hat{r}}$ and $E^{\hat{\theta}}$ are depicted for different values of the BH's charge. Here, too, as the charge increases, the values of the electric field components increase. In the right panel of Fig. 4, the electric field components $E^{\hat{r}}$ and $E^{\hat{\theta}}$ are depicted for different values of the BH's spin parameter. Here, it can be inferred that as the spin increases, the values of the electric field components $E^{\hat{r}}$ decrease and $E^{\hat{\theta}}$ increase.

Figure 5 presents the electric and magnetic field lines depicted within the Cartesian coordinate system. In the left panel of Fig. 5, the electric field is depicted using blue and black lines. The blue arrows, representing $E^{\hat{r}}$ and $E^{\hat{\theta}}$, are

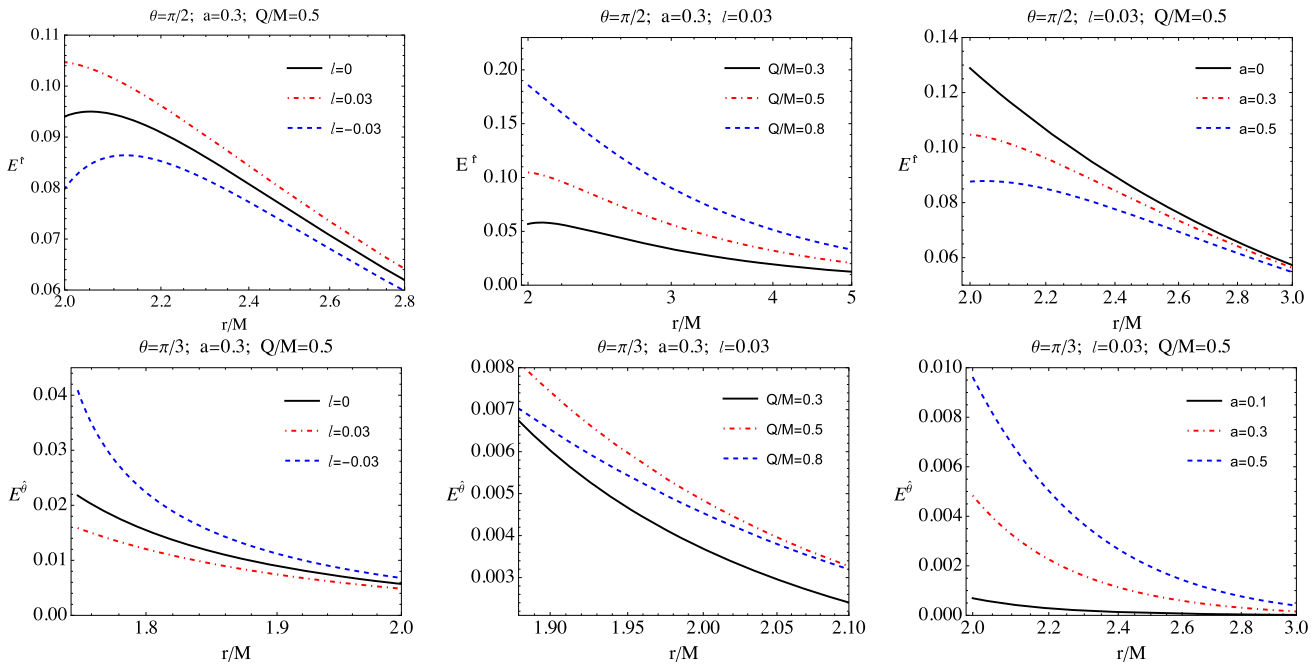

Fig. 4 Radial dependence of the electric field components $E^{\hat{\alpha}}$ around a charged rotating BH in KR gravity. Bottom row (left to right): $E^{\hat{\theta}}$ for $\theta = \pi/3$. Top row (left to right): $E^{\hat{r}}$ for $\theta = \pi/2$

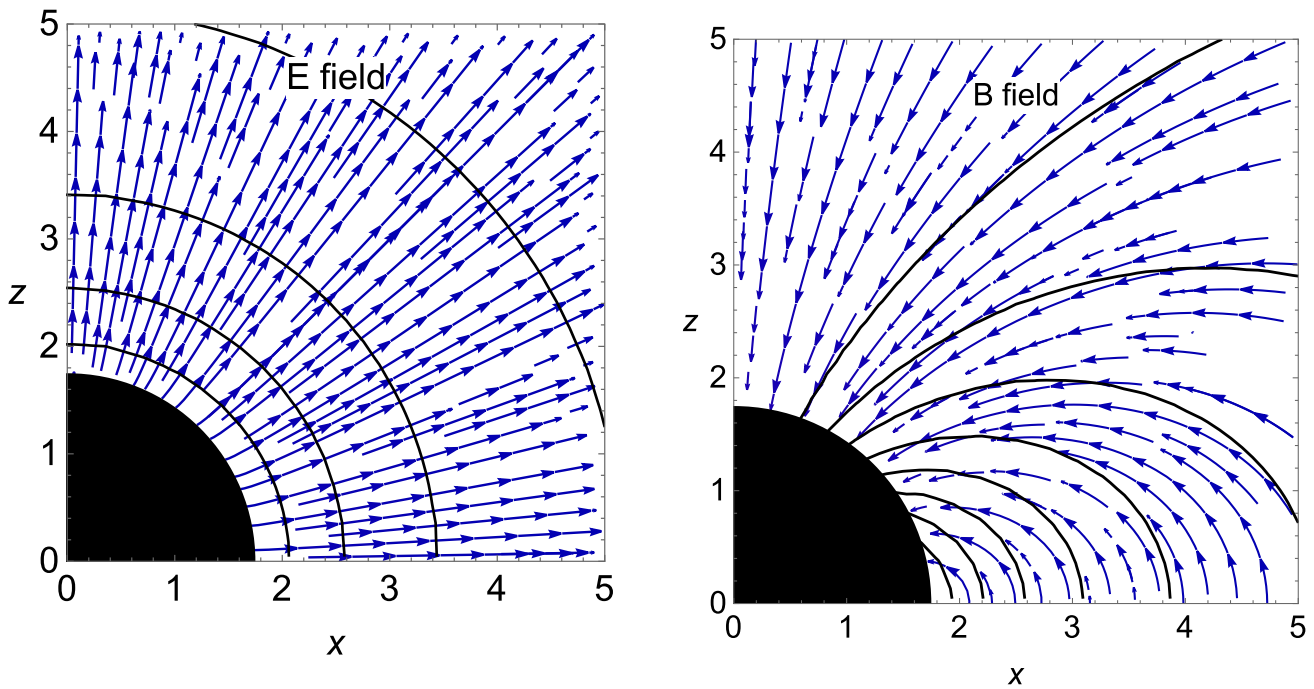

Fig. 5 Structure of the electric (left panel) and magnetic (right panel) fields around a charged rotating BH in KR gravity. We have set $Q/M = 0.5$, $M = 1$, $r_h = 1.75M$ $l = 0.03$ and $a = 0.3$.

stremplots of the electric field. The black lines represent the A_t component of the electromagnetic field, which also contributes to generating the electric field. In the right panel, the magnetic field is illustrated using blue and black lines. The blue arrows, depicting $B^{\hat{r}}$ and $B^{\hat{\theta}}$, are also streamplots of the magnetic field. The black lines represent the A_ϕ component, which also contributes to the production of the magnetic field.

5 Charged particle motion

In this section, we investigate the motion of charged particles in the spacetime of a charged rotating BH in KR gravity, under the influence of the electromagnetic field derived in Sect. 4. The gravitational and electromagnetic fields govern the dynamics of charged particles, the rotation of the BH, and the electromagnetic forces arising from its charge Q and the KR parameter l. We use the Hamilton-Jacobi formalism to analyze this, which provides a robust framework for studying particle trajectories in curved spacetime.

The specific electric charge parameter q quantifies the interaction between a charged test particle and an external electromagnetic field, significantly influencing its motion in magnetized astrophysical BHs. It is defined as $q = e/m$ where e is the charge of the test particle and m is the mass of the particle.

The Hamilton–Jacobi equation for a charged test particle with mass m and electric charge e in the presence of an electromagnetic field is given by [64,65]:

$$g^{\alpha\beta}\left(\frac{\partial S}{\partial x^\alpha}+eA_\alpha\right)\left(\frac{\partial S}{\partial x^\beta}+eA_\beta\right)=-m^2, \tag{63}$$

where S is the action. Due to the stationarity and axisymmetry of the spacetime, characterized by the timelike Killing vector $\xi^\alpha_{(t)} = (1,0,0,0)$ and the azimuthal Killing vector $\xi^\alpha_{(\phi)} = (0,0,0,1)$, the action can be separated as [66–68]:

$$S=-\mathcal{E}t+\mathcal{L}\phi+S(r,\theta), \tag{64}$$

where $\mathcal{E}$ and $\mathcal{L}$ are the conserved energy and angular momentum of the particle, respectively, which are normalized to the particle's rest energy mc^2, and $S(r,\theta)$ depends on the radial and polar coordinates.

Substituting these into the Hamilton–Jacobi equation and solving for the equations of motion, we obtain:

$$\frac{dt}{d\tau}=\frac{(\mathcal{E}+qA_t)r^2}{\Delta-a^2}, \tag{65}$$

$$\left(\frac{dr}{d\tau}\right)^2=\frac{\Delta}{r^2}\Big[-1+\frac{(\mathcal{E}+qA_t)^2r^2}{\Delta-a^2} -\left(r^2+a^2\left(1+\frac{a^2-\Delta}{r^2}\right)\right)\left(\frac{(\mathcal{L}-qA_\phi)r^2}{(r^2+a^2)^2-a^2\Delta}\right)^2 +2a\left(1+\frac{a^2-\Delta}{r^2}\right)\frac{(\mathcal{E}+qA_t)(\mathcal{L}-qA_\phi)r^4}{(\Delta-a^2)[(r^2+a^2)^2-a^2\Delta]}\Big], \tag{66}$$

$$\frac{d\phi}{d\tau}=\frac{(\mathcal{L}-qA_\phi)r^2}{(r^2+a^2)^2-a^2\Delta}, \tag{67}$$

where τ is the proper time.

To study the radial motion, we define an effective potential V_{eff} such that:

$$\left(\frac{dr}{d\tau}\right)^2+V_{\text{eff}}=\mathcal{E}. \tag{68}$$

We can write the variables in a separate form in the Hamilton–Jacobi equation. The radial motion of the particle can then be defined by

$$\begin{aligned} g_{rr}\dot{r}^2 &= \alpha\mathcal{E}^2+\delta\mathcal{E}+\gamma \\ &= \left[\mathcal{E}-V^+_{\text{eff}}(r)\right]\left[\mathcal{E}-V^-_{\text{eff}}(r)\right] \end{aligned} \tag{69}$$

and $V_{\text{eff}}(r)$ for the circular motion ($\dot{r}=0$) of charged magnetized particles has the form

$$V^\pm_{\text{eff}}=\frac{-\delta\pm\sqrt{\delta^2-4\alpha\gamma}}{2\alpha}, \tag{70}$$

where $\alpha = g^{tt}$ with $\delta = -2qA_tg^{tt}-g^{t\phi}\left(qA_\phi+\mathcal{L}\right)$,

$$\gamma = 1+g^{\phi\phi}(qA_\phi+\mathcal{L})^2+qA_\phi g^{t\phi}(qA_t+\mathcal{L})+q^2A_t^2g^{tt}.$$

Moving forward, we will concentrate on test particles possessing positive energy, thereby focusing on the effective potential $V_{\text{eff}} = V_+$.

Figure 6 illustrates the radial dependence of the effective potential, which shows how the parameters a, Q, and l influence potential barriers and stable orbits. Upper panel of Fig. 6 illustrates the radial dependence of the effective potential for the radial motion of test particles for different values of the spin parameter a in the case of $l = 0.03$, $Q/M = 0.5$, and a constant specific angular momentum $\mathcal{L} = 4.3M$ with $q = 0.1$. From the graph, it can be concluded that as the spin parameter a increases, the effective potential value increases. In the lower panel of Fig. 6 depicts the radial dependence of the effective potential for different values of the specific electric charge parameter q in the case of $l = 0.03$, $Q/M = 0.5$, and $\mathcal{L} = 4.3M$, with a fixed spin parameter $a = 0.3$. The graph shows that the effective potential also increases as the specific electric charge parameter q decreases.

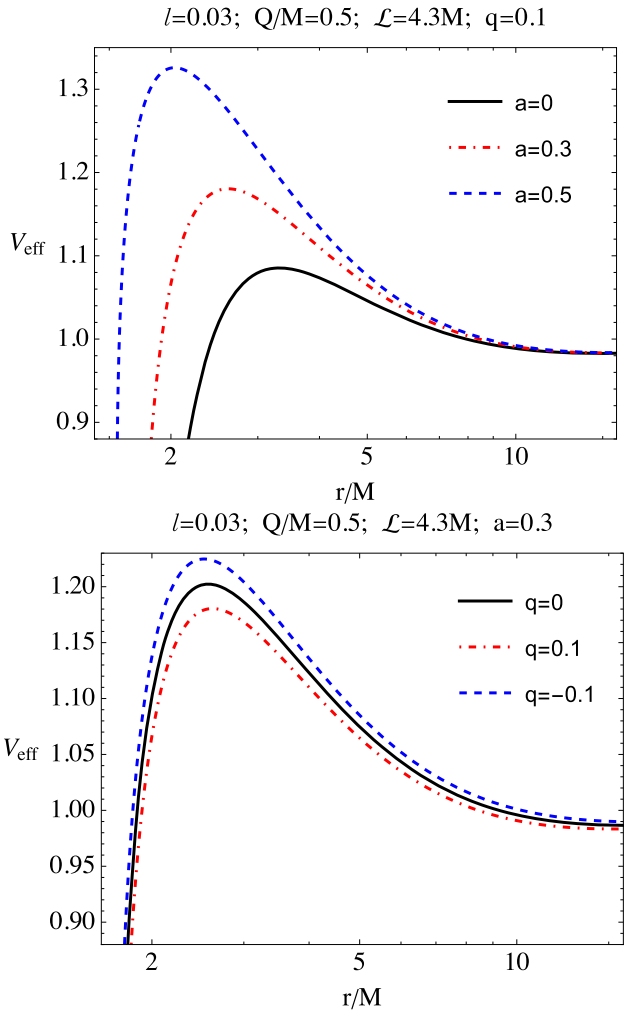

Fig. 6 Radial dependence of the effective potential V_{eff} for a charged particle in the spacetime of a rotating KR BH. Top: V_{eff} for $l = 0.03$ with $q = 0.1$ and $Q/M = 0.5$. Bottom: V_{eff} for $l = 0.03$ and $a = 0.3$

5.1 Stable circular orbits

Subsequently, we examine the circular orbits of test particles around a rotating charged BH in gravity with a background KR field based on the conditions provided below. For circular orbits, we impose the conditions [69]

$$\mathcal{E} = V_{\text{eff}}\,, \qquad \frac{dV_{\text{eff}}}{dr} = 0. \tag{71}$$

Solving these numerically (owing to the complexity of analytical expressions), we determine the energy $\mathcal{E}_c$ and the angular momentum $\mathcal{L}_c$ for charged particles in circular orbits. These are functions of r, a, Q, l, and q, with distinct solutions depending on the sign of the charge relative to the magnetic field orientation.

Figure 7 displays the radial dependence of $\mathcal{E}_c$ and $\mathcal{L}_c$, highlighting that higher values of Q and l increase the angular momentum required to maintain circular orbits, while the radius of the ISCO decreases with increasing q, aligning with the trends observed in [40,70]. Figure 7 illustrates the radial distribution of the specific energy ($\mathcal{E}$) and specific angular momentum ($\mathcal{L}$) for the circular orbits of test particles. The upper left panel of Fig. 7 shows the effect of the spin parameter a on the specific energy, considering $Q/M = 0.5$, $l = 0.03$, and $q = 0.1$. The graph indicates that as the spin parameter a increases, the specific energy $\mathcal{E}$ also decreases. The upper right panel of Fig. 7 illustrates the influence of the specific electric charge parameter q on $\mathcal{E}$, assuming $Q/M = 0.5$, $l = 0.03$, and $a = 0.3$. The graph shows that positive values of q increase the specific energy, while negative values decrease it. The lower left panel of Fig. 7 depicts the effect of the spin parameter a on angular momentum $\mathcal{L}$. The graph suggests that as the spin parameter a increases, the angular momentum $\mathcal{L}$ also decreases. The lower right panel of Fig. 7 illustrates the effect of the specific electric charge parameter q, showing that an increase in q leads to a rise in angular momentum $\mathcal{L}$.

5.2 Innermost stable circular orbits

The ISCO is the smallest radius at which a charged test particle can maintain a stable circular trajectory around a BH before collapsing into the event horizon due to gravitational instability. In the context of a charged rotating BH in KR gravity, the ISCO is influenced by the BH's rotation parameter a, charge Q, the KR field parameter l, and the specific electric charge parameter q. This subsection analyzes the ISCO's dependence on these parameters, building on the formalism established in Sect. 5 for charged particle motion.

To determine the ISCO, we use the conditions for stable circular orbits derived from the effective potential V_{eff} (Eq. 68). Specifically, a circular orbit requires $\mathcal{E} = V_{\text{eff}}$ and $\frac{dV_{\text{eff}}}{dr} = 0$, while stability demands that the second derivative satisfies $\frac{d^2V_{\text{eff}}}{dr^2} = 0$ at the ISCO radius r_{ISCO}. The complexity of the metric and electromagnetic field in KR gravity precludes a simple analytical solution, so we solve these conditions numerically, parameterizing the specific energy $\mathcal{E}_{\text{ISCO}}$ and angular momentum $\mathcal{L}_{\text{ISCO}}$ as functions of r_{ISCO}, a, Q, l, and q.

Figure 8 illustrates the dependence of the ISCO parameters on the BH rotation a and the specific electric charge q, with fixed values $Q/M = 0.5$ and $l = 0.03$. The top row shows the ISCO radius r_{ISCO} as a function of a (left) and q (right). As the rotation parameter a increases, r_{ISCO} decreases, consistent with trends observed in Kerr-like spacetimes. Similarly, increasing q, indicating stronger electromagnetic interaction, reduces r_{ISCO}, as the Lorentz force enhances the particle's ability to resist gravitational collapse,

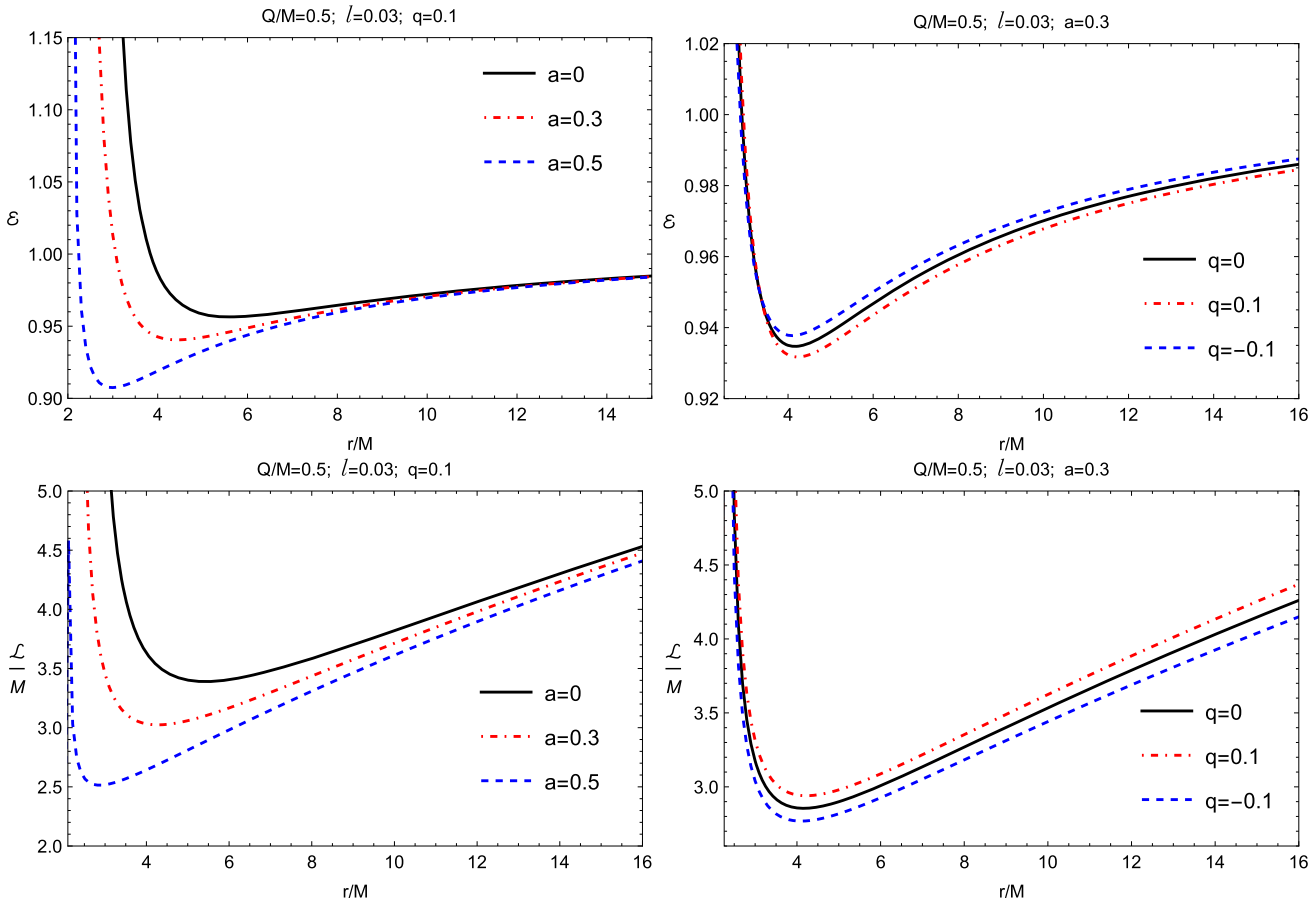

Fig. 7 Energy and angular momentum of charged particles in circular orbits around a rotating KR BH. Top row (left to right): Energy $\mathcal{E}_c$ for $q = 0.1$, $\mathcal{E}_c$ for $a = 0.3$. Bottom row (left to right): Angular momentum $\mathcal{L}_c$ for $q = 0.1$, $\mathcal{L}_c$ for $a = 0.3$. The parameters are $Q/M = 0.5$ and $l = 0.03$

aligning with findings for charged particles in magnetized BH environments.

The middle row of Fig. 8 depicts the specific angular momentum $\mathcal{L}_{\rm ISCO}$ versus a (left) and q (right). Higher a values increase $\mathcal{L}_{\rm ISCO}$, as faster rotation demands greater angular momentum to counterbalance the frame-dragging effect. Likewise, increasing q elevates $\mathcal{L}_{\rm ISCO}$, particularly for positive values, due to the additive contribution of the electromagnetic force to the particle's orbital dynamics. For negative q (opposite charge orientation), $\mathcal{L}_{\rm ISCO}$ may decrease, reflecting a repulsive interaction that reduces the required angular momentum.

The bottom row shows the specific energy $\mathcal{E}_{\rm ISCO}$ as a function of a (left) and q (right). An increase in a raises $\mathcal{E}_{\rm ISCO}$. The specific electric charge q also reduces $\mathcal{E}_{\rm ISCO}$ values. The KR parameter l introduces a unique modification compared to Kerr–Newman BHs ($l = 0$). As l increases, the lapse function Δ shifts, typically reducing $r_{\rm ISCO}$ and increasing both $\mathcal{L}_{\rm ISCO}$ and $\mathcal{E}_{\rm ISCO}$ due to the amplified gravitational and electromagnetic effects. This behavior underscores the KR field's role in enhancing the BH's influence on orbiting particles, a distinction from standard general relativity solutions. These results highlight the interplay of rotation, charge, and the KR field in shaping the ISCO, offering insights into the stability of accretion disks and particle dynamics near astrophysical BHs. The trends align with prior studies on modified gravity BHs, yet including l and q provides a novel perspective, potentially observable through astrophysical signatures like X-ray emissions from the accretion disk.

6 Collision of charged particles near a rotating charged BH in KR gravity

In this section, we explore the dynamics of charged particle collisions near the event horizon of a charged rotating BH in KR gravity. Such collisions are particularly interesting because they can lead to ultra-high-energy outcomes, potentially observable in astrophysical contexts, where BHs act as natural particle accelerators [71–73]. The energy released in these interactions is quantified by the center-of-mass energy $\mathcal{E}_{cm}$, which depends on the conserved quantities of the par-

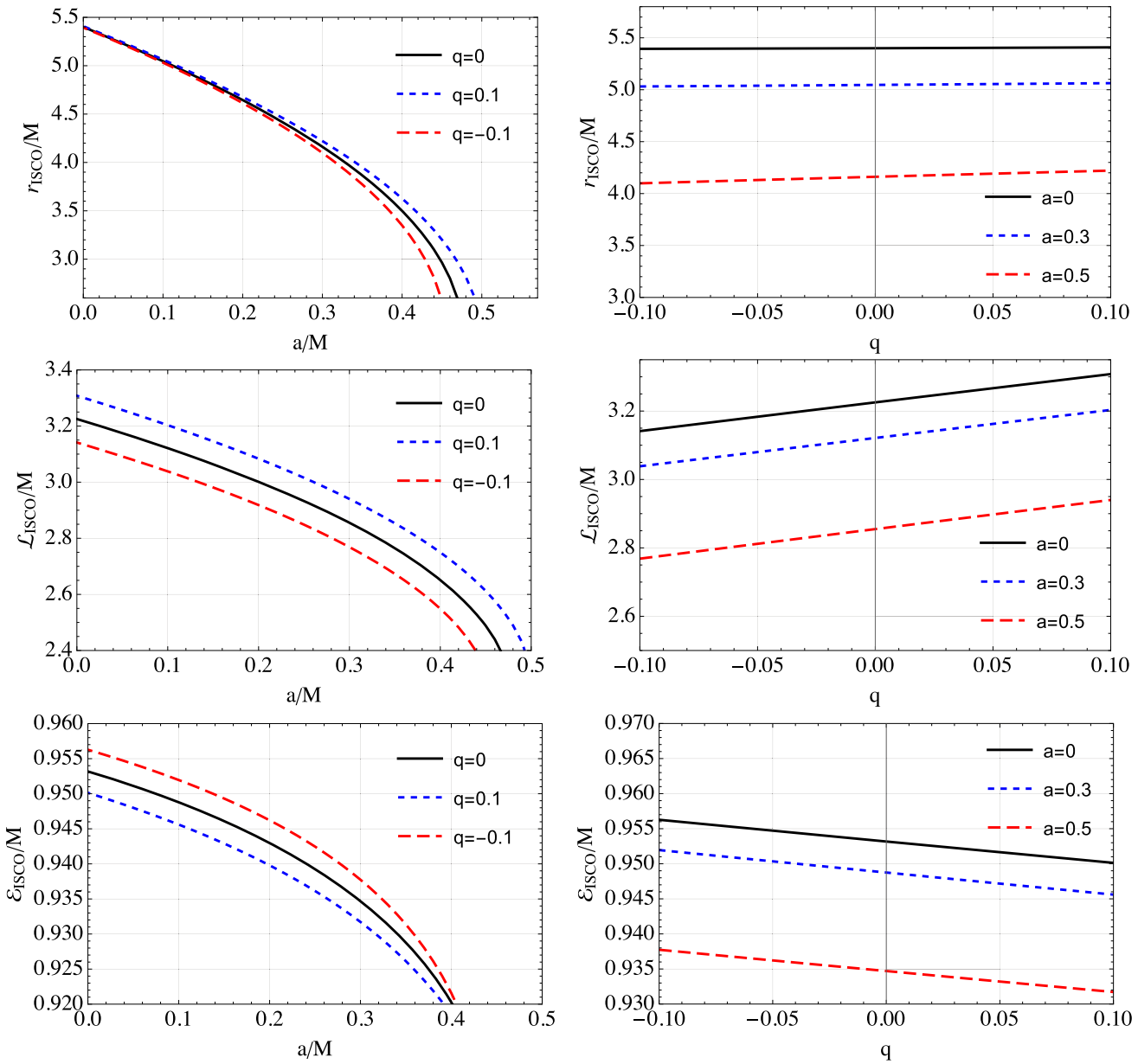

Fig. 8 Dependence of innermost stable circular orbit (ISCO) parameters on BH rotation a and parameter q for $Q/M = 0.5$ and $l = 0.03$. Top row (left to right): ISCO radius r_{ISCO} vs. a, r_{ISCO} vs. q. Middle row (left to right): angular momentum $\mathcal{L}_{ISCO}$ vs. a, $\mathcal{L}_{ISCO}$ vs. q. Bottom row (left to right): energy $\mathcal{E}_{ISCO}$ vs. a, $\mathcal{E}_{ISCO}$ vs. q. We have set $Q/M = 0.5$; $l = 0.03$

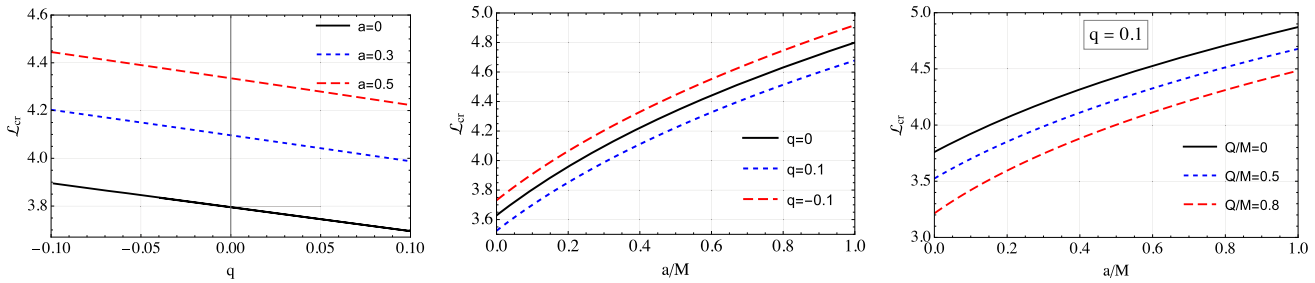

Fig. 9 The dependence of the critical angular momentum of a magnetized particle moving around a charged BH on the BH's spin (a), its charge (Q), and the specific electric charge parameter (q). We have set $Q/M = 0.5$; $l = 0.03$

ticles and the spacetime geometry modified by the KR field. For two charged particles with masses m_1 and m_2, charges q_1 and q_2, and four-momenta p_1^μ and p_2^μ, the center-of-mass energy is defined as [74,75]:

$$\mathcal{E}_{cm}^2 = (p_1^\mu + p_2^\mu)(p_{1\mu} + p_{2\mu}) = m_1^2 + m_2^2 + 2g_{\mu\nu}p_1^\mu p_2^\nu. \tag{72}$$

The four-momentum of a charged particle is given by $p^\mu = mu^\mu$, with $u^\mu = dx^\mu/d\tau$ derived from the equations of motion in Sect. 5. Numerical analysis reveals that $\mathcal{E}_{cm}$ grows unbounded as the collision point approaches r_h, particularly when the angular momentum of a particle is tuned to the critical value $\mathcal{L}_{cr}$. This behavior mirrors the Bañados–Silk–West (BSW) effect, but the presence of Q and l introduces additional dependencies, as explored in modified gravity frameworks. The influence of the electromagnetic field is significant for charged particles, as the Lorentz force modifies their trajectories and affects the energy extraction process [76,77]. For oppositely charged particles ($q_1 = -q_2$), the interaction with A_t can enhance relative velocities, leading to an increase in $\mathcal{E}_{cm}$ [78]. These results indicate that charged rotating KR BHs can act as efficient particle accelerators, potentially influencing high-energy astrophysical phenomena such as gamma-ray bursts [79,80] or the production of cosmic rays [81].

6.1 Critical angular momentum of colliding charged particles

The energy extraction efficiency during charged particle collisions near the event horizon of a rotating charged BH in KR gravity hinges critically on the angular momentum of the particles involved. Specifically, the critical angular momentum $\mathcal{L}_{cr}$ represents the threshold value at which the trajectory of a particle transitions from being captured by the BH to narrowly escaping or orbiting near the horizon, a condition crucial for achieving ultrahigh center-of-mass energies $\mathcal{E}_{cm}$ as described in the Bañados–Silk–West (BSW). In this subsection, we derive and analyze $\mathcal{L}_{cr}$ for charged particles under the influence of the BH's charge Q, rotation parameter a, and the KR field parameter l, leveraging the equations of motion from Sect. 5 and the spacetime geometry from Sect. 2.

For a charged particle with mass m and charge e, the radial motion is governed by the effective potential V_{eff}, as derived in Eq. (68) of Sect. 5. The critical angular momentum $\mathcal{L}_{cr}$ corresponds to the value of $\mathcal{L}$ at which a particle can reach the event horizon r_h (where $\Delta = 0$) with zero radial velocity ($u^r = 0$), poised at the brink of capture. Setting $(dr/d\tau)^2 = 0$ in Equation (30) of Sect. 6 and evaluating at $r = r_h$ yields the critical condition. The two solutions correspond to co-rotating (+) and counter-rotating (−) orbits relative to the BH's rotation [82,83]. For particles incoming from infinity with normalized energy $\mathcal{E} = 1$, the dependence of $\mathcal{L}_{cr}$ on Q, a, and l highlights the enhanced efficiency of energy extraction in KR gravity compared to standard Kerr–Newman spacetimes.

The dependence of $\mathcal{L}_{cr}$ on a, Q, and l is illustrated in Fig. 9 (top row), where we plot $\mathcal{L}_{cr}$ as a function of rotation parameter a for varying q parameter values. In the left panel of Fig. 9, the values of the critical angular momentum are depicted for different values of the BH's spin parameter a. It can be observed from the figure that as the spin parameter increases, the critical angular momentum also increases. In the middle panel of Fig. 9, the values of the critical angular momentum are depicted for different values of the specific electric charge parameter. It can be observed from the figure that as the q parameter increases, the critical angular momentum $\mathcal{L}_{cr}$ decreases. In the right panel of Fig. 9, the values of the critical angular momentum are depicted for different values of the BH's charge. It can be inferred from the figure that as the charge Q increases, the critical angular momentum $\mathcal{L}_{cr}$ decreases.

6.2 Center of mass energy of charged particles in different scenarios

In the context of collisions, one particle with $\mathcal{L}_1 \approx \mathcal{L}_{cr}$ orbiting near r_h collides with another particle incoming from infinity ($\mathcal{E}_2 = 1$, $\mathcal{L}_2 < \mathcal{L}_{cr}$). As $r \to r_h$, the denominator Δ in the four-velocity components approaches zero, causing u^t and u^ϕ to diverge, thereby boosting $\mathcal{E}_{cm}$. The critical nature of $\mathcal{L}_{cr}$ ensures maximal relative velocity between the colliding particles, a key factor in the BSW effect. Numerical results (see Fig. 10) confirm that tuning $\mathcal{L}_1$ to $\mathcal{L}_{cr}$ maximizes $\mathcal{E}_{cm}$, with enhancements driven by larger Q and l, consistent with the stronger electromagnetic and gravitational effects in KR gravity. These findings underscore the pivotal role of $\mathcal{L}_{cr}$ in high-energy collisions, providing a pathway to probe the extreme physics of charged, rotating Kerr black holes. Future work could explore backreaction effects or the impact of charge ratios (q/Q) on $\mathcal{L}_{cr}$, further refining the astrophysical implications of these accelerators.

Figure 10 illustrates $\mathcal{E}_{cm}$ as a function of r for varying a, Q and l. In the top left panel of Fig. 10, we can observe the dependence of the collision energy of two positively charged particles on the radial coordinate for different values of electric charge. As the electric charge of the particles increases, the collision energy also decreases. Similarly, in the top right panel of Fig. 10, the dependence of the collision energy of a negatively charged particle with a positively charged particle on the radial coordinate is shown. Here, too, the collision energy decreases as the charges increase. On the left side of the middle panel, we depict the collision energy of two positively charged particles with the same charge value for integer values of the BH charge. As the BH charge increases,

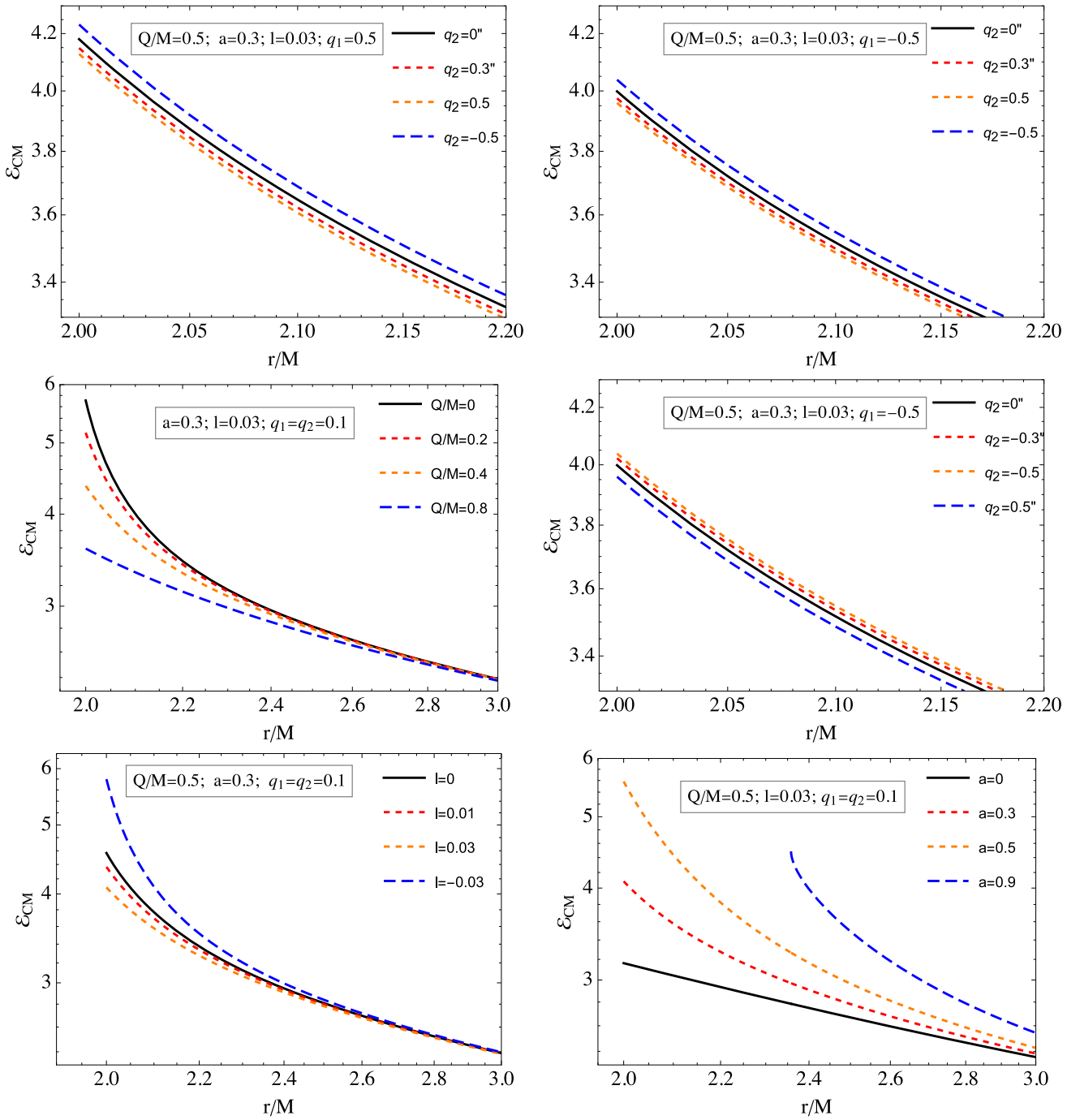

Fig. 10 Radial dependence of the center-of-mass energy $\mathcal{E}_{cm}$ for charged particle collisions near the BH, with parameters a, Q/M, and varying l

the collision energy decreases. On the right side of the middle panel, we illustrate the collision energy of two negatively charged particles for integer values of the second particle's charge, while keeping the charge of the first particle constant. As the charge of the second particle increases, the collision energy increases. On the left side of the bottom panel, we depict the collision energy values for two particles with the same charge for different values of the KR field parameter l. The KR parameter l increases, and the collision energy $\mathcal{E}_{cm}$ decreases. It can also be observed from the right side of the bottom panel that as the BH rotation parameter a increases, the collision energy $\mathcal{E}_{cm}$ decreases.

7 Conclusion

In this study, we have conducted a comprehensive analysis of the dynamics of charged particles in the vicinity of a charged rotating BH within the framework of KR gravity. By deriving the spacetime geometry and electromagnetic field configuration, we have elucidated the combined effects of the BH's mass M, charge Q, rotation parameter a, and the KR field parameter l. The incorporation of the KR field, a rank-2 antisymmetric tensor field rooted in string theory, introduces significant modifications to the gravitational and electromagnetic interactions compared to the standard Kerr–Newman solution in general relativity. Our results underscore the profound impact of these modifications on the event horizon, ergosphere, electromagnetic field structure, circular orbits, and high-energy particle collisions, providing new insights into the physics of extreme gravitational environments. The spacetime metric, derived using the Janis–Newman algorithm adapted to the KR framework, reveals that the KR parameter l amplifies the gravitational and electromagnetic effects, reducing the event horizon radius and compressing the ergosphere. This alteration allows charged particles to orbit closer to the BH, impacting the ISCOs. Through the Hamilton–Jacobi formalism, we analyzed the effective potential. We determined the energy and angular momentum of charged particles in circular orbits, demonstrating that both Q and l enhance the angular momentum required for stable orbits while reducing the ISCO radius. These findings have direct implications for the dynamics of accretion disks, potentially influencing observable signatures such as X-ray emissions from astrophysical BHs. The electromagnetic field, computed using Giampieri and tetrad formulations, exhibits a modified vector potential due to the KR field, with the factor $(1-l)^{-1}$ amplifying the field strength. The electric and magnetic field components, derived in the ZAMO frame, show a clear dependence on Q, a, and l, with positive l values reducing field magnitudes, as illustrated in Figs. 3 and 4. This modified field structure has a significant impact on the motion of charged particles, as the Lorentz force introduces additional complexities compared to uncharged scenarios. A key focus of this work was the investigation of high-energy particle collisions near the event horizon, where the center-of-mass energy $\mathcal{E}_{cm}$ can become unbounded, particularly when one particle's angular momentum approaches the critical value $\mathcal{L}_{cr}$. Our numerical analysis (Fig. 10) confirms that the BSW effect is enhanced by the BH's charge and the KR parameter, making charged rotating KR BHs efficient natural particle accelerators. The dependence of $\mathcal{E}_{cm}$ on Q, a, and l, as well as the specific electric charge q, underscores the potential for these systems to produce high-energy astrophysical phenomena, such as gamma-ray bursts or ultra-high-energy cosmic rays, which could be detectable by observatories like Fermi-LAT [84] or the Cherenkov Telescope Array [85]. Looking ahead, several avenues for future research emerge from this study. First, the impact of the KR parameter l on gravitational wave signatures from BH mergers warrants further exploration, as deviations from general relativity could be probed using data from LIGO-Virgo [86] or future detectors like LISA [87]. Second, the backreaction effects of charged particle motion on the spacetime geometry could provide deeper insights into the stability of orbits and the validity of the test particle approximation. Third, observational constraints on l could be established by analyzing X-ray emission profiles from accretion disks around astrophysical BHs, leveraging data from telescopes like Chandra [88], XMM-Newton [89], or the upcoming Athena mission [90]. Additionally, investigating the polarization properties of electromagnetic radiation or the effects of KR gravity on BH shadows, as observed by the Event Horizon Telescope, could offer empirical tests of the theory. A critical question for future work is how the KR field influences the thermodynamics of BHs, particularly in the context of Hawking radiation or entropy modifications due to the antisymmetric tensor field. In other words, the results of the study underscore the rich phenomenology of charged rotating BHs in KR gravity, revealing their potential as laboratories for probing fundamental physics. The interplay of gravitational, electromagnetic, and KR field effects not only enriches our theoretical understanding but also opens new pathways for connecting theoretical predictions with astrophysical observations. By refining our understanding of these systems and their observable signatures, we can better constrain modified gravity theories and explore the interface between string-inspired models and real-world astrophysical phenomena.

Data Availability Statement This manuscript has no associated data. [Authors' comment: Data sharing does not apply to this paper, as no datasets were generated or analyzed during this study.].

Code Availability Statement The manuscript has no associated code/software. [Author's comment: Code/Software sharing does not apply to this paper, as no code/software was generated or analyzed during the current study.].

Funded by SCOAP[3].

References

1. C.M. Will, Living Rev. Relativ. **17**, 1 (2014). https://doi.org/10.12942/lrr-2014-4
2. EHT Collaboration et al., Astrophys. J. Lett. **875**, L1 (2019). https://doi.org/10.3847/2041-8213/ab0ec7
3. K. Akiyama et al., Event horizon telescope. Astrophys. J. Lett. **930**, L12 (2022). https://doi.org/10.3847/2041-8213/ac6674. arXiv:2311.08680
4. S.U. Khan, J. Ren, Phys. Dark Universe **30**, 100644 (2020). https://doi.org/10.1016/j.dark.2020.100644
5. EHT Collaboration, Astrophys. J. Lett. **910**, L13 (2021). https://doi.org/10.3847/2041-8213/abe4de
6. S. Jumaniyozov, S. Ullah Khan, J. Rayimbaev, I. Ibragimov, A. Abdujabbarov, Z.C.V. Stuchlík, Phys. Rev. D **112**, 044068 (2025). https://doi.org/10.1103/bl45-hbjm
7. S.U. Khan, J. Ren, Chin. J. Phys. **78**, 141 (2022). https://doi.org/10.1016/j.cjph.2022.06.017. arXiv:2012.07639 [gr-qc]
8. D.J. Gross, J.A. Harvey, E. Martinec, R. Rohm, Phys. Rev. Lett. **54**, 502 (1985). https://doi.org/10.1103/PhysRevLett.54.502
9. C.-Y. Yang, K.-J. He, X.-X. Zeng, L.-F. Li, (2025). arXiv:2508.07393 [gr-qc]
10. D.S.J. Cordeiro, E.L.B. Junior, J.T. S.S. Junior, F.S.N. Lobo, M.E. Rodrigues, D. Rubiera-Garcia, L.F.D. da Silva, H.A. Vieira, (2025). arXiv:2503.12048 [gr-qc]
11. F. Hosseinifar, A.A.A. Filho, M.Y. Zhang, H. Chen, H. Hassanabadi (2024), arXiv:2407.07017 [gr-qc]
12. B. Toshmatov, K. Mavlyanov, B. Abdulazizov, A. Mamadjanov, F. Atamurotov, Ann. Phys. **458**, 169450 (2023). https://doi.org/10.1016/j.aop.2023.169450
13. O. Rahimov, B. Toshmatov, Y. Vyblyi, A. Akhmedov, B. Abdulazizov, Phys. Dark Universe **44**, 101483 (2024). https://doi.org/10.1016/j.dark.2024.101483
14. B. Altschul, Q.G. Bailey, V.A. Kostelecký, Phys. Rev. D **81**, 065028 (2010). https://doi.org/10.1103/PhysRevD.81.065028
15. F. Ahmed, A. Al-Badawi, İ. Sakallı, (2025). arXiv:2508.03226 [gr-qc]
16. E. Sucu, İ Sakall, Phys. Rev. D **111**, 064049 (2025). https://doi.org/10.1103/PhysRevD.111.064049
17. S. Mardonov, J. Rayimbaev, F. Abdulkhamidov, E. Karimbaev, B. Abdulazizov, Class. Quantum Gravity **42**, 115004 (2025). https://doi.org/10.1088/1361-6382/adcb83
18. R. Kumar, S.G. Ghosh, A. Wang, Phys. Rev. D **101**, 104001 (2020). https://doi.org/10.1103/PhysRevD.101.104001
19. Y. Sekhmani, A. Baruah, S.K. Maurya, J. Rayimbaev, M. Altanji, I. Ibragimov, S. Muminov, (2025). arXiv:2507.19088 [gr-qc]
20. Y. Ma, S. Zheng, H. Li, B. Li, Nucl. Phys. B **1009**, 116732 (2024). https://doi.org/10.1016/j.nuclphysb.2024.116732
21. M. Asrat, (2024). https://doi.org/10.1007/JHEP08(2025)135. arXiv:2410.07580 [hep-th]
22. D.K. Bekov, T.A. Akhunov, O.A. Burkhonov, N.R. Alimova, Astrophys. Bull. **79**, 15 (2024). https://doi.org/10.1134/S1990341323600278
23. M.D. Seifert, Phys. Rev. Lett. **105**, 201601 (2010). https://doi.org/10.1103/PhysRevLett.105.201601. arXiv:1008.0324 [hep-th]
24. P.H. Cox, B.C. Harms, S. Hou, Phys. Rev. D **93**, 044014 (2016). https://doi.org/10.1103/PhysRevD.93.044014
25. R.C. Pantig, A. Övgün, Á. Rincón, Phys. Dark Universe **49**, 102029 (2025). https://doi.org/10.1016/j.dark.2025.102029. arXiv:2505.17947 [gr-qc]
26. S. Chandrasekhar, *The Mathematical Theory of Black Holes* (Oxford University Press, Oxford, 1983)
27. B. Carter, Phys. Rev. **174**, 1559 (1968). https://doi.org/10.1103/PhysRev.174.1559
28. M. Mangut, H. Gürsel, İ Sakallı, Chin. Phys. C **49**, 065106 (2025). https://doi.org/10.1088/1674-1137/adbacf. arXiv:2504.02108 [gr-qc]
29. V.F. Mukhanov, H.A. Feldman, R.H. Brandenberger, Phys. Rep. **215**, 203 (1992). https://doi.org/10.1016/0370-1573(92)90044-Z
30. B. Turimov, S. Usanov, Y. Khamroev, Phys. Dark Universe **48**, 101876 (2025). https://doi.org/10.1016/j.dark.2025.101876. arXiv:2502.11185 [gr-qc]
31. S. Nojiri, S.D. Odintsov, Phys. Rev. D **68**, 123512 (2005). https://doi.org/10.1103/PhysRevD.68.123512
32. S. Capozziello, M. De Laurentis, Phys. Rep. **509**, 167 (2011). https://doi.org/10.1016/j.physrep.2011.09.003
33. V.A. Derkach, C. Trunk, J.R. Yusupov, D.U. Matrasulov, J. Phys. A Math. Gen. **58**, 345201 (2025). https://doi.org/10.1088/1751-8121/adf787. arXiv:2410.10232 [math-ph]
34. F. Botirov, S. Nuritdinov, Open Astron. **30**, 144 (2021). https://doi.org/10.1515/astro-2021-0019
35. C. Bambi, Rev. Mod. Phys. **89**, 025001 (2017). https://doi.org/10.1103/RevModPhys.89.025001
36. M.M. Suleimanov, M.U. Nosirov, H.T. Yusupov, A. Chaves, G.R. Berdiyorov, K.Y. Rakhimov, Phys. B **714**, 417484 (2025). https://doi.org/10.1016/j.physb.2025.417484. arXiv:2411.02896 [cond-mat.mes-hall]
37. E.T. Newman, A.I. Janis, J. Math. Phys. **6**, 915 (1965). https://doi.org/10.1063/1.1704350
38. M. Bañados, J. Silk, S.M. West, Phys. Rev. Lett. **103**, 111102 (2009). https://doi.org/10.1103/PhysRevLett.103.111102
39. V.P. Frolov, Phys. Rev. D **85**, 024020 (2012). https://doi.org/10.1103/PhysRevD.85.024020
40. A. Abdujabbarov, B. Ahmedov, A. Hakimov, Phys. Rev. D **88**, 024008 (2013). https://doi.org/10.1103/PhysRevD.88.024008
41. A. AlBadawi, S. Shaymatov, I. Sakallı, Eur. Phys. J. C **84**, 825 (2024). https://doi.org/10.1140/epjc/s10052-024-13205-7. arXiv:2408.09228 [gr-qc]
42. Z. Stuchlík, J. Schee, Class. Quantum Gravity **27**, 215017 (2010). https://doi.org/10.1088/0264-9381/27/21/215017
43. B. Mashhoon, Phys. Rev. D **31**, 290 (1985). https://doi.org/10.1103/PhysRevD.31.290
44. M. Zahid, O. Yunusov, C. Shen, J. Rayimbaev, S. Muminov, Phys. Dark Universe **47**, 101734 (2025). https://doi.org/10.1016/j.dark.2024.101734
45. R. Penrose, Rivista del Nuovo Cimento **1**, 252 (1969)
46. F.U. Botirov, S.N. Nuritdinov, A.E. Ashurov, Astron. Rep. **67**, 448 (2023). https://doi.org/10.1134/S1063772923050013
47. S.N. Nuritdinov, A.A. Muminov, F.U. Botirov, Astron. Astrophys. Trans. **32**, 83 (2021). https://doi.org/10.48550/arXiv.2002.09310. arXiv:2002.09310 [astro-ph.GA]
48. J.D. Schnittman, Astrophys. J. **806**, 264 (2015). https://doi.org/10.1088/0004-637X/806/2/264
49. K. Tan, X.G. Lan, Chin. Phys. C **49**, 075104 (2025). https://doi.org/10.1088/1674-1137/adc3fc. arXiv:2503.16800 [gr-qc]
50. K. Myrzakulov, O. Donmez, M. Koussour, S. Muminov, E. Davletov, J. Rayimbaev, (2025). arXiv:2501.03388 [astro-ph.CO]
51. S.S. Kutlimuratov, N.B. Otojanova, I.U. Tadjibaev, Ukr. J. Phys. **69**, 367 (2024). https://doi.org/10.15407/ujpe69.6.367
52. S. Kutlimuratov, N. Otojanova, I. Tadjibaev, K. Tillaboev, EUREKA Phys. Eng. **4**, 3 (2024). https://doi.org/10.21303/2461-4262.2024.003416
53. Z.-Q. Duan, J.-Y. Zhao, K. Yang, Eur. Phys. J. C **84**, 798 (2024). https://doi.org/10.1140/epjc/s10052-024-13188-5. arXiv:2310.13555 [gr-qc]
54. M.M. Gohain, D.J. Gogoi, K. Bhuyan, P. Phukon, (2025). arXiv:2508.18053 [astro-ph.CO]
55. S.G. Ghosh, S.U. Islam, S.D. Maharaj, Phys. Scr. **99**, 065032 (2024). https://doi.org/10.1088/1402-4896/ad4833. arXiv:2307.11611 [gr-qc]

56. P. Li, J.-H. Yang, (2025). arXiv:2501.12586 [gr-qc]
57. A.G. Suvorov, P. Bargueño, Phys. Rev. D **112**, 044027 (2025). https://doi.org/10.1103/ljjy-v4m1. arXiv:2507.23250 [gr-qc]
58. M. Enayatinia, B. Mirza, M. Moradzadeh, M.E. Khuzani, Int. J. Geom. Methods Mod. Phys. **22**, 2550023 (2025). https://doi.org/10.1142/S0219887825500239
59. B. Toshmatov, Z. Stuchlík, B. Ahmedov, Eur. Phys. J. Plus **132**, 98 (2017). https://doi.org/10.1140/epjp/i2017-11373-4. arXiv:1512.01498 [gr-qc]
60. D.S.J. Cordeiro, E.L.B. Junior, J.T. S.S. Junior, F.S.N. Lobo, M.E. Rodrigues, D. Rubiera-Garcia, L.F. D. da Silva, H.A. Vieira, Free-falling test particles in a charged kalb-ramond black hole: gravitational doppler effect and tidal forces (2025). arXiv:2503.12048 [gr-qc]
61. E. Harold, Gravity Res. Found. Essays (2015). https://doi.org/10.1007/s10714-015-1860-1
62. H. Erbin, (2018) arXiv:1410.2602
63. E.T. Newman, E. Couch, K. Chinnapared, A. Exton, A. Prakash, R. Torrence, J. Math. Phys. **6**, 918 (1965). https://doi.org/10.1063/1.1704351
64. C.A. Benavides-Gallego, A. Abdujabbarov, D. Malafarina, B. Ahmedov, C. Bambi, Phys. Rev. D **99**, 044012 (2019). https://doi.org/10.1103/PhysRevD.99.044012
65. S. Jumaniyozov, S.U. Khan, J. Rayimbaev, A. Abdujabbarov, S. Urinbaev, S. Murodov, Eur. Phys. J. C **84**, 964 (2024). https://doi.org/10.1140/epjc/s10052-024-13351-y
66. A. Abdujabbarov, B. Ahmedov, Phys. Rev. D **81**, 044022 (2010). https://doi.org/10.1103/PhysRevD.81.044022
67. J. Rayimbaev, S. Jumaniyozov, M. Umaraliyev, A. Abdujabbarov, Universe **8**, 496 (2022). https://doi.org/10.3390/universe8100496
68. B. Rahmatov, M. Zahid, S.U. Khan, J. Rayimbaev, I. Ibragimov, Z. Yuldoshev, A. Dauletov, S. Muminov, Chin. Phys. C **49**, 075105 (2025). https://doi.org/10.1088/1674-1137/adc188
69. S.U. Khan, J. Ren, Chin. J. Phys. **70**, 55–68 (2021). https://doi.org/10.1016/j.cjph.2020.08.027
70. S. Jumaniyozov, S. Murodov, J. Rayimbaev, I. Ibragimov, B. Madaminov, S. Urinbaev, A. Abdujabbarov, Eur. Phys. J. C **85**, 797 (2025). https://doi.org/10.1140/epjc/s10052-025-14522-1
71. M. Zahid, J. Rayimbaev, N. Kurbonov, S. Ahmedov, C. Shen, A. Abdujabbarov, Eur. Phys. J. C **84**, 706 (2024). https://doi.org/10.1140/epjc/s10052-024-13061-5
72. T. Jacobson, T.P. Sotiriou, Phys. Rev. Lett. **104**, 021101 (2010). https://doi.org/10.1103/PhysRevLett.104.021101
73. J. Rayimbaev, U. Eshimbetov, B. Majeed, A. Abdujabbarov, A. Abduvokhidov, B. Abdulazizov, A. Xalmirzayev, Chin. Phys. C **48**, 055104 (2024). https://doi.org/10.1088/1674-1137/ad2060
74. I. Nishonov, J. Rayimbaev, S.U. Khan, M. Zahid, T. Tolibjanov, I. Ibragimov, Eur. Phys. J. C **85**, 325 (2025). https://doi.org/10.1140/epjc/s10052-025-13945-0
75. S.U. Khan, M. Shahzadi, J. Ren, Phys. Dark Universe **26**, 100331 (2019). https://doi.org/10.1016/j.dark.2019.100331
76. W. Cao, X. Wu, J. Lyu, Eur. Phys. J. C **84**, 435 (2024). https://doi.org/10.1140/epjc/s10052-024-12804-8. arXiv:2404.19225 [gr-qc]
77. S.U. Khan, U. Uktamov, J. Rayimbaev, A. Abdujabbarov, I. Ibragimov, Z.-M. Chen, Eur. Phys. J. C **84**, 203 (2024). https://doi.org/10.1140/epjc/s10052-024-12567-2
78. S. Jumaniyozov, S. Khan, J. Rayimbaev et al., Eur. Phys. J. C **84**, 291 (2024). https://doi.org/10.1140/epjc/s10052-024-12605-z
79. T. Piran, Rev. Mod. Phys. **76**, 1143 (2005). https://doi.org/10.1103/RevModPhys.76.1143
80. M. Zahid, F. Sarikulov, C. Shen, J. Rayimbaev, K. Badalov, S. Muminov, Chin. J. Phys. **91**, 45 (2024). https://doi.org/10.1016/j.cjph.2024.07.008
81. K. Kotera, A.V. Olinto, Ann. Rev. Astron. Astrophys. **49**, 119 (2011). https://doi.org/10.1146/annurev-astro-081710-102620
82. E. Hackmann, V. Kagramanova, J. Kunz, C. Lämmerzahl, Phys. Rev. D **81**, 044020 (2010). https://doi.org/10.1103/PhysRevD.81.044020
83. S. Jumaniyozov, M. Zahid, M. Alloqulov, et al., Eur. Phys. J. C **85** (2025). https://doi.org/10.1140/epjc/s10052-025-13863-1
84. S. Abdollahi et al., Astrophys. J. **976**, 203 (2024). https://doi.org/10.3847/1538-4357/ad64c5. arXiv:2501.08015 [astro-ph.HE]
85. S. Ravikularaman, F. Riehn, D. Elsaesser, in *39th International Cosmic Ray Conference* (2025). arXiv:2508.01354 [astro-ph.HE]
86. A.G. Abac et al., (LIGO Scientific (VIRGO, KAGRA)) (2025). arXiv:2508.20721 [gr-qc]
87. A.W. Criswell, S. Banagiri, J. Lawrence, L. Schult, S. Rieck, S.R. Taylor, V. Mandic (2025). arXiv:2508.20308 [astro-ph.IM]
88. J. Zhao, C.O. Heinke, P.S. Shternin, W.C.G. Ho, D.D. Ofengeim, D. Patnaude, (2025). arXiv:2508.15161 [astro-ph.HE]
89. C. Spinelli, A. Veronica, F. Pacaud, T.H. Reiprich, K. Migkas, W. Xu, M.E. Ramos-Ceja, Astron. Astrophys. **700**, A220 (2025). https://doi.org/10.1051/0004-6361/202346294. arXiv:2506.19718 [astro-ph.CO]
90. N. Covas, I. Matute, S. Amarantidis, J. Afonso, G. Lanzuisi, A. Comastri, S. Marchesi, C. Pappalardo, R. Carvajal, P. Papaderos, (2025). arXiv:2504.10731 [astro-ph.GA]